Bioorganic Chemistry 90 (2019) 103055

Contents lists available at ScienceDirect

Bioorganic Chemistry

journal homepage: www.elsevier.com/locate/bioorg

Anticancer properties of N-alkyl-2, 4-diphenylimidazo [1, 2-a] quinoxalin-1-amine derivatives; kinase inhibitors

Zahra Rezaei[a], Mir Mahdi Didehvar[b], Mohammad Mahdavi[c], Homa Azizian[d], Haleh Hamedifar[e], Eman H.M. Mohammed[f], Sayednaser Ostad[g], Mohsen Amini[h,*]

[a] Department of Medicinal Chemistry, Faculty of Pharmacy, Tehran University of Medical Sciences, 14176 Tehran, Iran
[b] School of Chemistry, University College of Science, University of Tehran, PO Box 14155-6455, Tehran, Iran
[c] Endocrinology and Metabolism Research Center, Endocrinology and Metabolism Research Institute, Tehran University of Medical Sciences, Tehran, Iran
[d] Department of Medicinal Chemistry, School of Pharmacy-International Campus, Iran University of Medical Sciences, Tehran, Iran
[e] CinnaGen Medical Biotechnology Research Center, Alborz University of Medical Sciences, Karaj, Iran
[f] Department of Chemistry, Faculty of Sciences, Menoufia University, Shebin EI-Koam, Egypt
[g] Department of Toxicology & Pharmacology, Faculty of Pharmacy, Tehran University of Medical Sciences, Tehran, Iran
[h] Department of Medicinal Chemistry, Faculty of Pharmacy and Drug Design and Development Research Center, The Institute of Pharmaceutical Sciences (TIPS), Tehran, Iran

ARTICLE INFO

Keywords:
Synthesis
Quinoxalin
Anticancer
Kinase inhibitor
Docking

ABSTRACT

Structure activity correlation revealed that the quinoxaline ring is a satisfactory backbone for anticancer activity and a specific functional group at position 1 and 2 can improve the activity. In this basis, besides quinoxaline, imidazoles as potential anticancer agents were used as a supplementary agents for cancer treatment.

In this paper, a new series of N-alkyl-2, 4-diphenylimidazo [1, 2-a] quinoxalin-1-amine derivatives were synthesized in a simple and efficient step. The products are fully characterized by 1H NMR, ^{13}C NMR, FT-IR, HRMS, and CHN elemental analysis. Several starting materials with different functionalities have been used for the synthesis of the final products with high isolated yields. The biological activities of the synthesized compounds were evaluated in kinase inhibition and cytotoxic activity in several cancerous cell lines. All compounds (6) were evaluated for inhibition of the cell proliferation using 4 cancerous cell lines. Five of the more active compounds were studied for determination of $IC50_{\%}$. Compounds 6(32–34) showed good activity on some of cancerous cell lines.

The results showed that compound **6–32** has the highest biological activity (IC_{50}% 9.77 for K562 cell line). An IC_{50}% value of 15.84 μM was observed for **6–34.** Furthermore **6–34** exhibited inhibition of ABL1 and c-Src kinases with an IC50% value of 5.25 μM and 3.94 μM respectively**.** Docking simulation was performed to position active synthesized compounds **6–32**, **6–33**, and **6–34** over the ABL1 active site in two different wild-type (DFG-in and DFG-out motif conformer) and T315I mutant to determine the probable binding orientation, conformation and mode of interaction. According to docking study, the docked location in wild type forms is similar and can be found near the P-loop region while in the case of T315I mutant form, the compounds have a distinct docked location which is close to the αC helix and activation loop. Also, it concluded the role of R_1 substituent on phenyl ring produced higher interaction energy. Additionally, the detailed inter-molecular energy and types of non-bonding interaction of these compounds over the wild-type and mutant form of ABL1.

1. Introduction

Cancer, as an abnormal cell growth disease, is one of the most important human diseases that is reported as the second cause of death [1]. Between several clinical protocols for cancer treatment, chemotherapy is interesting in aspect of molecular targeting and is a strategy in cancer treatment [2]. One way for cancer treatment is inhibition of cancerous cell growth in which Kinase inhibition is an efficient approach due to its important role in cell growth [3]. Kinases are the largest and the most important families of proteins that have been known as an enzyme for catalysis phosphate transfer, are a key target for controlling the cell activities such as cell survival and death, cellular distinction, transcription, metabolisms, and duplication processes [4]. This protein have been targeted for different drug therapy in

* Corresponding author.
E-mail address: moamini@tums.ac.ir (M. Amini).

https://doi.org/10.1016/j.bioorg.2019.103055
Received 10 November 2018; Received in revised form 27 March 2019; Accepted 6 June 2019
Available online 10 June 2019

a wide range of diseases including inflammation and cardiovascular diseases, CNS disorders and cancer. In cancer, the importance of kinase targeting could be referred to recently identified over-express kinase receptors in various tumor but not in normal cells. Therefore, it has been expected the chemical agents that have targeted kinases show low toxicity in normal organs. In structural aspects, a high similarity could be observed in different human kinases esp. in catalytic site, where is a connection part to bind with ATP. This part is including β-sheet in N-terminal, α-helix in C-terminal and Hing region. The more kinases inhibitors act in Hing region. Based on different substrates, protein kinases have been divided to several branches that may be phosphorylated the phenolic group of tyrosine or react with other amino acids such as threonine and serine. Recently, a new kinase has been identified that phosphorylates the nitrogen of histidine. Among of them, the role of tyrosine kinases in pathogenesis of cancer has been extensively studied. Mutation in the related gene has been distinguished in a large amounts of human tumors. Now today, 90 gene of tyrosine kinase have been discovered that most of them are related to receptor tyrosine kinase. The position of this receptors is cell membrane and act both enzyme and receptors. Based on the kinases domain, receptor tyrosine kinases have been categorized to several families. ErbB are the first family of receptor tyrosine kinase that its function is related to EGFR. The decreasing activity of EGFR causes to CNS disorders such as MS and Alzheimer's disease and the increasing activity of EFGR causes to cancer. This family includes four isoforms, $ErbB_{1-4}$ that have been inhibited by gefitinib, erlutinib, lapatiniband and vandetanib. All of them has 4-aminoquinazoline ring as core. The second family including sorafenib, sunitinib, razopanib inhibit VEGF and in conclusion, act in angiogenesis processes. Anaplastic lymphoma kinase inhibitors has been identified as third branches of kinases including crizotinib, ceritinib, and alectinib. Src family kinases has been categorized as non-receptor tyrosin kinases that are a family of nine diferent PTKs. In recent years development of Src kinase inhibitors led to discovery of several drugs such as anti-cancer agents, among of them; quinoxaline derivatives have gained considerable attention in several studies [5–8].

Quinoxaline is a heterocyclic compound containing benzene fused to a pyrazin ring. This class of organic compounds is a core for a large number of candidate kinase inhibitor agents [9–13].

Compounds A and B (Fig. 1) have been introduced as type $I_{1/2}$ and II Eph tyrosine kinase inhibitors [16]. The development of quinoxaline core fused to pyrazole ring leaded to present compounds C (Fig. 1) with considerable anti-cancer activity [42].

On the other hand imidazole derivatives have been studied vastly as anticancer agents. Some of the imidazole derivatives showed a little or no drug resistance by cancerous cell lines that is a promising source for cancer treatment [14–20]. Furthermore comound D (Fig. 1), a derivative of imidazo[1,5-a] quinoxaline showed a remarkable activity for IKK2 (IκB kinase) inhibition [15].

Docking methodologies asserted that binding imidazole derivatives to quinoxaline could increase its biological activity drastically via enhancement affinity of ligand to kinase protein that has been confirmed by experimental data [21,22].

The most oncogenic receptor kinases have low activity in normal cells but they are hyper-activated in malignant cells. Hence, targeting receptor kinase by inhibitors is very attractive in cancer drug

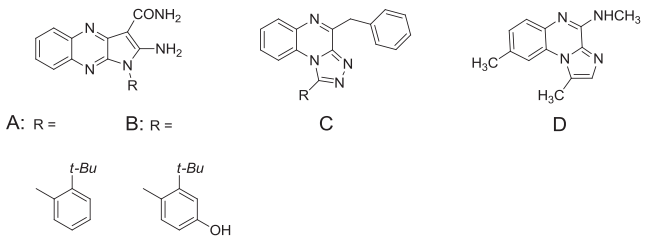

Fig. 1. Some quinoxaline derivatives having anticancer activity.

developments. Regarding the importance of the kinase inhibitors in cancer treatment, here by we report the synthesis of a novel series of imidazo[1,2-*a*]quinoxalin-1-amine derivatives and evaluation of their kinase inhibitory activities.

2. Results and discussion

In the current work, a new simple and efficient process is suggested for producing imidazole-quinoxaline derivatives. A glance at the previous literature revealed that there are different synthesis route for quinoxaline derivatives synthesis. Most of the synthetic strategies are based on the reaction of *o*-phenylenediamine with aldehydes, 2-nitroaniline, 1,2-diketone compounds, alkynes, and epoxide compounds [23–31].

In this paper, N-methyl-2, 4-diphenylimidazo [1, 2-a] quinoxalin-1-amine derivatives were synthesized in two steps. The first step consists of cyclization reaction of *o*-phenylenediamine with sodium cyanide and benzaldehyde derivatives to form 3-phenylquinoxalin-2-amine intermediate (3). The reaction was performed at 50 °C and was catalyzed with 4Å molecular sieve (MS). Then, 3-phenylquinoxalin-2-amine intermediate and isocyanate was prepared in the presence of a catalytic amount of ammonium hydrochloride. The second step of the reaction is performed in the solvent free conditions. Stirring the reaction mixture in high temperature can lead to higher isolated yields. The reaction steps are presented in Scheme 1.

2.1. Chemistry

For finding the optimal reaction conditions, both of the reaction steps were studied in different conditions. Optimization of the reactions was studied using different temperatures and reaction time in several solvents. For the first step, the best yield was obtained in 50 °C for 5 h using DMF as solvent. More details of the optimized results are presented in Table 1. The reaction has yielded the desired product in all protic and aprotic solvents. Our experiences showed that increasing the reaction temperature did not have any positive effects on the yields.

The second step of the reaction was performed in different reaction conditions using various solvents to obtain the optimal reaction conditions. Using different solvents and in solvent free conditions proved that, the best performance could be obtained in solvent free conditions. In addition, the reaction was tested in different temperatures and reaction times. The results showed that 150 °C temperature and 24 h reaction time are the best reaction conditions. Detailed results of the optimization reactions are presented in Table 2.

Multicomponent reactions were investigated in optimal conditions. Various benzaldehydes with electron-donating/electron-withdrawing functionalities were used in both reaction steps. As a result, the desired products were achieved successfully. The structure of the products is shown in Table 3.

2.2. Biological evaluation

The cytotoxic effect of the products was studied on three cancerous cell lines; HEK-293, MB-468 and CCRF for 24 h and 72 h and normal cell lineas at a concentration of 50 μM. The results were presented in Table 4. The activity of the compounds was compared with Doxorubicin and Dasatinib (5 μM) as reference drugs. Compounds **6–32, 6–33**, and **6–34** were the most active compounds in three cancerous cell lines after 24 and 72 h. In addition, compounds **6–6** and **6–7** significantly inhibit the cell proliferation of HEK-293 cells after 72 h incubation. For the three more active compounds, the cytotoxcicity was studied on normal cell line, NIH-3T3, at 50 μM.

For cancerous cell lines, In the cases of more than 75% viability the results did not present or showed as "In" (inactive) in Table 4.

Cytotoxicity cell-based assays were conducted on human B leukemia

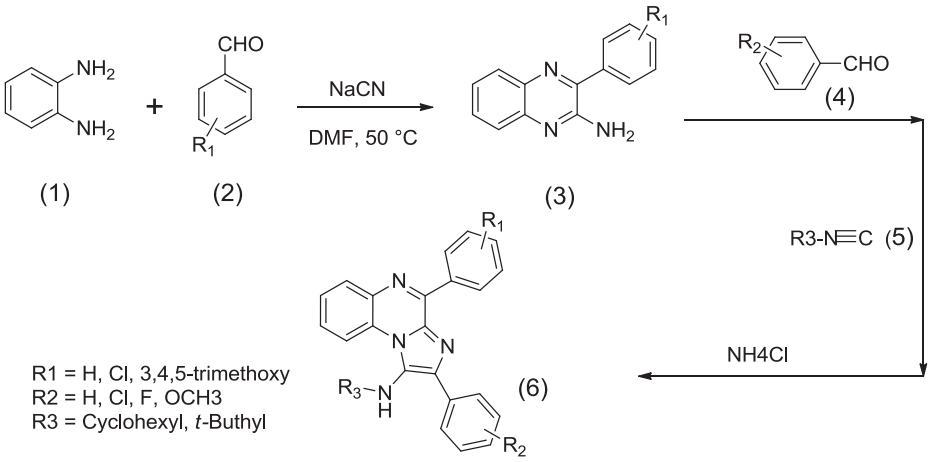

Scheme 1. Synthesis steps of *N*-alkyl-2,4-diphenylimidazo[1,2-*a*]quinoxalin-1-amine derivatives.

Table 1
Optimization results for the preparation of 3-phenylquinoxalin-2-amine intermediate.[a]

Entry	Solvent	Temperature (°C)	Time (h)	Yield (%) [b]
1	Toluene	50	4	70
2	MeOH	50	4	25
3	EtOH	50	4	35
4	DMSO	50	4	53
5	DMF	25	4	0
6	DMF	40	4	10
7	DMF	50	1	35
8	DMF	50	2	50
9	DMF	50	3	65
10	DMF	50	4	85
11	DMF	50	5	85
12	DMF	50	6	84
13	DMF	70	4	30
14	DMF	100	4	25
15	CH_2Cl_2	50	4	40
16	CH_3Cl	50	4	37

[a] Reaction conditions: *o*-phenylenediamine (5 mmol), benzaldehyde (5 mmol), sodium cyalide (6 mmol), 4Å molecular sieve (100 mg), solvent (10 mL).
[b] Isolated yield.

Table 2
Optimization results for the preparation of 3-phenylquinoxalin-2-amine intermediate.[a]

Entry	Solvent	Temperature (°C)	Time (h)	Yield (%)[b]
1	DMF	150	24	19
2	Toluene	150	24	15
3	H_2O	150	24	8
4	H_2O-MeOH (1:1)	150	24	10
5	H_2O- EtOH (1:1)	150	24	12
6	H_2O-MeOH (2:1)	150	24	14
7	H_2O- EtOH (2:1)	150	24	15
8	Solvent free	20	24	0
9	Solvent free	50	24	10
10	Solvent free	95	24	43
11	Solvent free	120	24	55
12	Solvent free	150	6	25
13	Solvent free	150	18	60
14	Solvent free	150	24	90
15	Solvent free	150	36	90
16	Solvent free	170	24	88

[a] Reaction conditions: 3-phenylquinoxalin-2-amine (2 mmol), benzaldehyde (2 mmol), isocyanide (2 mmol), ammonium chloride (0.25 mmol).
[b] Isolated yield.

cell lines (BV- 173, Creative Bioarray # CSC-C0203), bone marrow lymphoma (K652, ATTC # CCL-243), breast epithelial (MCF 10A, ATCC # CRL-10317), and mammary gland/breast (MDA-MB-468, ATCC # HTB-132) cell lines. BV-173 cell line is an example of Philadelphia chromosome (Ph1) + chronic myeloid leukemia derived from the peripheral blood of a 45-year-old man with CML in blast crisis in 1980. K562 is an example of bone marrow leukemia cells. As Table 5, compounds **6–32, 6–33,** and **6–34** exhibited anti-proliferative activities in the concentration range tested with IC_{50} values of 9.77–15.84 μM against K-562 cells. Other compounds did not show any significant anti-proliferative activities at the lower than 25 μM. The effect of concentrations on the inhibitory activity of K-562 was presented in Fig. 2. Values are derives from 2 indipendent experiments, the standard deviation were also note.

The inhibitory property of the most cytotoxic compounds was studied as kinase inhibitors. The inhibitory activity of compounds **6–5**, **6–14**, **6–32, 6–33,** and **6–34** were studied on three kinases: ABL1, c-Src and LCK. The results are presented in Table 6. Compounds **6–5, 6–14, 6–32**, and **6–33** did not show any significant kinase inhibition in the lower than 125 μM. Compound **6–34** showed inhibition against ABL1 and c-Src with IC_{50} values of about 5.25 and 3.93 μM, respectively. Compound **6–34** did not show inhibition of LCK at a concentration of 125 μM, but inhibited the proliferation by approximately 32% inhibition at 125 μM.

2.3. Molecular docking

2.3.1. Evaluation of docking procedure

Before docking, it is necessary to verify the reliability of the docking study. The three native ligands were extracted from the X-ray structures of ABL1 (PDB entry: 2gqg, 4zoq, 3qrj) and redocked into their corresponding protein active site pockets according to the above docking protocol. The superimposed lowest energy poses for redocking results over the co-crystalized ligands with their corresponding interactions were shown in Fig. 3(a–c). The RMSD of the re-docked and co-crystalized ligands over related 2gqg, 4zoq, and 3qrj were 1.6 Å, 1.1 Å, and 0.6 Å, respectively, which are considered as successfully docked procedure. As a result, the validity of docked parameters is reasonable in order to predict the related co-crystalized structures. Table 6 indicates energy data and types of interaction of each ligand- protein complex.

2.3.2. Binding interaction and poses analysis of the active compounds

For study the molecular docking, the most active compounds (**6–14**, and **6-(32–34)**) were chosen. Furthermore, compounds **6–7** and **6–24** were selected for comparing the substitution effect on R_1 position. In the predicted binding mode obtained by docking studies, all the studied compounds were successfully docked into the corresponding binding

Table 3
The structure of compounds **6-(1–34)** and their isolated yield.

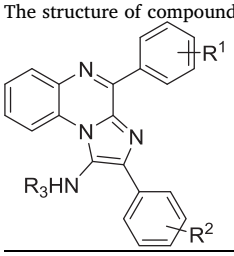

Compound	R_1	R_2	R_3	MW	Isolated yield (%)
6–1	4-Cl	4-Cl	Cyclohexyl	487.43	85
6–2	4-Cl	3,4,5-$(OMe)_3$	Cyclohexyl	543.06	90
6–3	4-Cl	3,4-$(OMe)_2$	Cyclohexyl	513.04	88
6–4	4-Cl	4-OMe	Cyclohexyl	483.01	91
6–5	4-Cl	4-F	Cyclohexyl	470.98	84
6–6	4-Cl	3,4,5-$(OMe)_3$	*t*-butyl	517.03	89
6–7	4-Cl	3,4-$(OMe)_2$	*t*-butyl	487.00	87
6–8	4-Cl	4-OMe	*t*-butyl	456.97	82
6–9	4-Cl	H	*t*-butyl	426.95	85
6–10	4-Cl	H	Cyclohexyl	452.99	86
6–11	4-Cl	4-Cl	*t*-butyl	461.39	89
6–12	3,4,5-$(OMe)_3$	3,4,5-$(OMe)_3$	Cyclohexyl	598.70	88
6–13	3,4,5-$(OMe)_3$	3,4,5-$(OMe)_3$	*t*-butyl	572.66	90
6–14	3,4,5-$(OMe)_3$	3,4-$(OMe)_2$	Cyclohexyl	568.67	91
6–15	3,4,5-$(OMe)_3$	3,4-$(OMe)_2$	*t*-butyl	542.64	87
6–16	3,4,5-$(OMe)_3$	4-OMe	Cyclohexyl	538.65	90
6–17	3,4,5-$(OMe)_3$	4-OMe	*t*-butyl	512.61	88
6–18	3,4,5-$(OMe)_3$	H	Cyclohexyl	508.62	89
6–19	H	3,4,5-$(OMe)_3$	Cyclohexyl	508.62	92
6–20	H	3,4,5-$(OMe)_3$	*t*-butyl	482.58	89
6–21	H	3,4-$(OMe)_2$	Cyclohexyl	478.60	90
6–22	H	3,4-$(OMe)_2$	*t*-butyl	452.56	86
6–23	H	H	Cyclohexyl	418.54	83
6–24	H	H	*t*-butyl	392.51	84
6–25	H	4-F	Cyclohexyl	436.53	85
6–26	H	4-F	*t*-butyl	410.50	89
6–27	H	4-OMe	Cyclohexyl	448.57	86
6–28	H	4-OMe	*t*-butyl	422.53	84
6–29	H	4-Cl	Cyclohexyl	452.99	85
6–30	H	4-Cl	*t*-butyl	426.95	82
6–31	2-OH-3-OMe	3,4,5-$(OMe)_3$	Cyclohexyl	554.65	70
6–32	2-OH-3-OMe	3,4,5-$(OMe)_3$	*t*-butyl	528.61	68
6–33	2-OH-3-OMe	3,4-$(OMe)_2$	Cyclohexyl	524.62	76
6–34	2-OH-3-OMe	3,4-$(OMe)_2$	*t*-butyl	498.58	72

pocket of ABL1. It can be found difference in docked location and orientation of compounds over the active site of DFG-in, DFG-out and mutant T315I forms of ABL1 (Fig. 4, Table 7). The docked location in wild type forms (DFG-in and DFG-out) is similar and can be found near the P-loop region of kinase active site (Fig. 4a, b) while in the case of T315I gatekeeper mutant form, the compounds have a distinct docked location which is close to the αC helix and activation loop (Fig. 4c). The different binding location in ABL1 mutant conformer could be a result of the long-range conformational impact of T315I mutation.

The docking results of synthesized compounds including; detailed intermolecular energy and the residues involving in the types of

Table 4
The cytotoxicity of more active synthesized compounds in three cancerous cell lines.

Cell line / Compounds	NIH-3T3 (% Viability)		MB-468, MTS (% Viability)		CCRF, MTS (% Viability)		HEK-293, MTS (% Viability)	
Entry	24	72	24	72	24	72	24	72
Cell	100	100	100	100	100	100	100	100
Water	98	97	107	121	103	96	101	96
DMSO	31	27	37	21	21	31	12	19
6–5	–	–	93	12	In	In	In	In
6–6	–	–	120	73	In	In	103	12
6–7	–	–	In	In	In	In	106	12
6–12	–	–	In	In	95	74	In	In
6–13	–	–	80	21	In	In	In	In
6–14	–	–	93	21	In	In	In	In
6–16	–	–	62	72	In	In	In	In
6–20	–	–	95	66	In	In	In	In
6–22	–	–	97	69	In	In	In	In
6–32	73	55	In	In	14	31	43	31
6–33	74	61	60	60	16	29	27	22
6–34	98	77	66	21	30	48	31	18
DOX (5 μM)	79	27	78	29	89	71	66	20
DAS (5 μM)	91	66	104	86	85	75	95	126

nonbonding interaction over DFG-in, DFG-out and mutant T315I form of ABL1 were presented in Tables 8–10, respectively. It can be observed that active compounds; **6-(32–34)** with 2-hydroxy-3-methoxy group on phenyl ring (R_1) have higher interaction energy over ABL1 than compound **6–24** which does not have R_1 group at mentioned position. As a result, the presence of R_1 substitution affects the ABL1 tyrosine kinase affinity. The 2-hydroxyl-3-methoxy substituention has the ability to produce essential H-bond and polar interaction with surrounding residues. Table 8 indicates that compounds **6-(32–34)** have higher interaction energy rather than dasatinib over DFG-in conformer of ABL1 which is quite compatible with the experimental results of higher viability percentage of applied cell line after treating of dasatinib rather than compounds **6-(32–34)** over hek-293, MB-468, and CCRF cell line (Table 4). Furthermore, Tables 8–10 show the interaction energy of active synthesized compounds **6-(32–34)** which is higher than the binding energy of staurosporin (−11.73, −13.12, −12.06, −9.41 kcal mol^{-1}, respectively) over DFG-in (2gqg) and mutant form (3qrj) (−13.01, −13.67, −12.49, −7.76 kcal mol^{-1}, respectively), while the electrostatic interaction energy of staurosporin is significantly higher than mentioned compounds (the electrostatic energy for **6-(32–34)**, and staurosporin over 2gqg are −0.18, −0.07, −0.25, and −1.62 kcal mol^{-1}, respectively and over 3qrj are −0.06, −0.07, −0.07, and −0.77 kcal mol^{-1}, respectively). This finding can be used to propose the outstanding role of electrostatic and polar interaction in tyrosine kinase binding affinity in active and mutant conformers of ABL1.

*2.3.3. Binding pose comparison of compound **6–34** and co-crystalized inhibitors over DFG-in, DFG out, and mutant variant of ABL1*

Fig. 5a shows binding interactions of compound **6–34** and dasatinib over ABL1 DFG-in. Compound **6–34** mainly occupies the adenine pocket by the two phenyl rings containing R_1 and R_2 substitutions, while the quinoxaline and trimethyl amine (R_3) group extend beyond the interlobe connector near the mouth of the active site and are solvent exposed. A total of three bonds is formed between compound **6–34** and the active ABL1. Two hydrogen bonds are formed to the Gln252 from P-loop ATP binding pocket of kinase through the 2-hydroxy-3-methoxy phenyl moiety which is not observed in ABL1:dasatinib. The other hydrogen bonds are made between a methoxy group of 3,4-dimethoxy phenyl and the backbone NH of Met318 in the loop linking *N*-lobe and C-lobe together. The remaining binding interactions are electrostatic interaction with Asp325 and Hydrophobic interaction of π-π *T*-shape, π-

Table 5
IC_{50} of the most active compounds in four cancerous cell lines.

Cell Viability	Compounds IC_{50} (μM)					
Cell Line	**6–5**	**6–14**	**6–32**	**6–33**	**6–34**	Staurosporine
BV-173	> 25	> 25	> 25	> 25	> 25	0.37 ± 0.02
K-562	> 25	> 25	9.77 ± 0.91	12.02 ± 1.45	15.84 ± 1.15	0.047 ± 0.008
MCF 10A	> 25	> 25	> 25	> 25	> 25	0.056 ± 0.004
MDA-MB-468	> 25	> 25	> 25	> 25	> 25	0.15 ± 0.04
NIH-3T3	> 25	> 25	> 25	> 25	> 25	0.09 ± 0.003

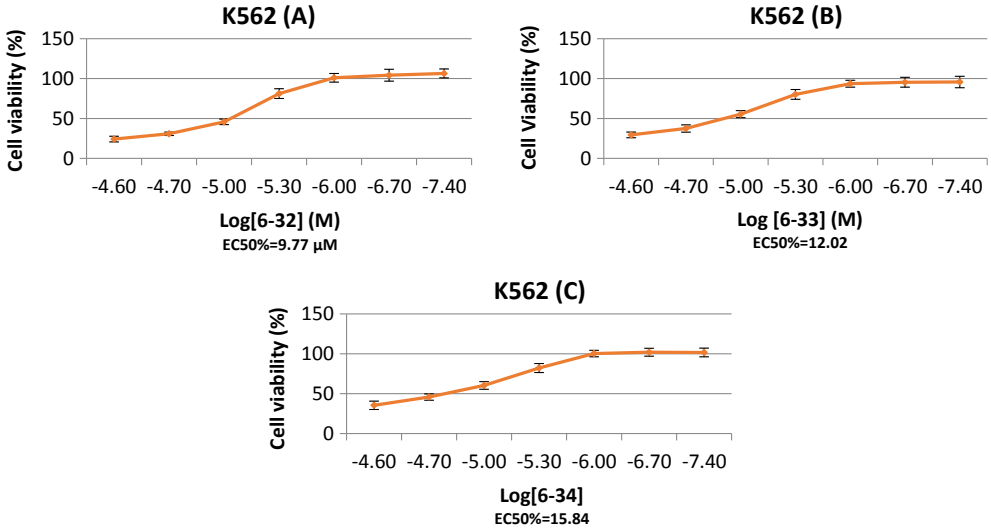

Fig. 2. Inhibitory activity of compounds (A) **6–32**; (B) **6–33**; and (C) **6–34** against K-562.

Table 6
Inhibitory activity of the products.

	Compound IC_{50} (μM)					
Kinases	**6–5**	**6–14**	**6–32**	**6–33**	**6–34**	Staurosporine
ABL1	> 125	> 125	> 125	> 125	5.25 ± 0.08	0.93 ± 0.01
c-Src	> 125	> 125	> 125	> 125	3.94 ± 0.05	0.038 ± 0.0045
LCK	> 125	> 125	> 125	> 125	> 125	0.036 ± 0.001

sigma, and π-alkyl with Tyr253, Leu370, and Leu348, respectively.

Compound **6–34** and dasatinib share different functionalities that bind in the pocket of the DFG-in motif. The main difference between compound **6–34** and dasatinib, therefore, is in their H-bonding pattern. Dasatinib makes two H-bonds with Thr315 and Tyr320 which are not obsevable for compound **6–34.**

Fig. 5b shows binding interactions of compound **6–34** and VX-280 over ABL1 DFG-out. Compound **6–34** with its dimethoxy phenyl part produced H-bonding interaction with the backbone NH of Gly383 from the DFG motif in the "out" conformation. Furthermore, the corresponding phenyl group stabilized at specific pocket by side chain of Lys271 via electrostatic anion-π interaction.

Also, Ala380 from the activation loop, Tyr353 and Val256 from the P-loop participate in hydrophobic interaction by π-alkyl, π-π stack and, π-alkyl interactions with compound **6–34**. Comparison of the ABL1: compound **6–34** and ABL1:VX-280 reveals that compound **6–34** can binds deeply into the active site and it occupies the selectivity pocket behind the gatekeeper residue Thr315 and the hydrophobic pocket induced by the DFG-out motif with the quinoxaline and 2-hydroxy-3-methoxy moiety, while VX-268 could not reach to that specific pocket with its piperazine and pieridine rings are near the mouth of the active site and are solvent exposed.

Fig. 5c,d represent binding interactions of compound **6–34** and DCC-2036 over ABL1 mutant variant. Compound **6–34** positioned in the kinase active site close to the αC helix motif in which the 2-hydroxy-3-methoxy phenyl ring and trimethyl amine substituents are solvent assailable parts with mentioned phenyl interacts Glu286 via π-anion electrostatic attraction. Additionally, the 3,4-dimethoxy moiety put deeply into the active site and produced H-bond interaction with Lys271 through its methoxy substitution. Also, the corresponding phenyl group and the quinoxaline ring stabilized between αC helix and activation loop with Phe382 from DFG motif (π-π stack) and Ala380, Ile315, Met290, Val299, and Leu298 via π-alkyl interaction. Similarly, DCC-2036 is in the same location as compound **6–34** and interacts Lys271 and Glu286 via H-bonding (Fig. 5d).

2.4. Molecular dynamic simulation

In order to carry out the movement of particles (atoms and molecules), molecular dynamics (MD) simulation has been applied over the period of 40 ns. The total energy of the top ranked complex accomplished by molecular dynamics simulation was discovered to be −95214.581 and −83268.453 kcal/mol for the wild type and T315I mutant variant, respectively.

Root mean square deviation (RMSD) is used to reveal the stability of protein structure by measuring the variation between the protein's backbones from its original to final conformation over 40 ns which defined as RMSD. The RMSD simulation showed that the wild type maintained an overall stability throughout the last 15 ns of simulation with higher fluctuation, stabilizing at an average of 2.7 Å, while the T315I mutant variant displayed lower fluctuations over the same period and its equilibration was not obtained during that time (Fig. 6).

the RMSF plot indicates the residues of both system fluctuate in low level of flexibility with the maximum quantity at 2.5 Å. Also, it depictes

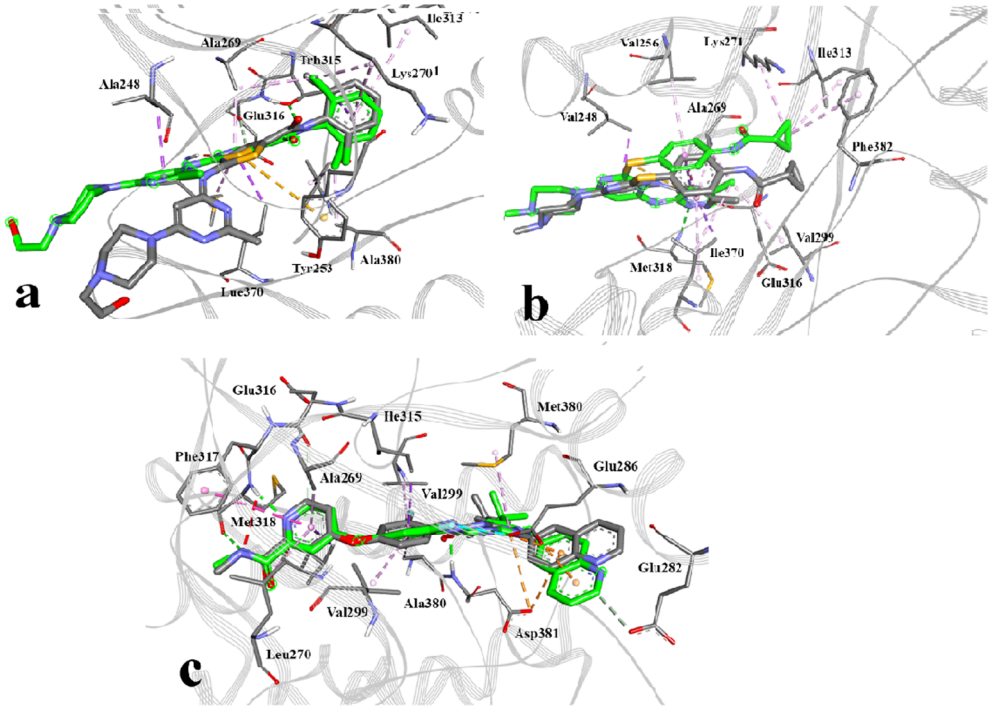

Fig. 3. Superimposed representation of re-docking lowest energy poses into the co-crystalized ligands dasatinib, VX-680, and DCC-2036 over 2gqg (a), 4zoq (b), 3qrj (c), respectively. Co-crystalized and redock ligands were shown in green and gray carbon atom color. Dash line in green, orange, yellow, pink, purple and pale pink are corresponding to H-bond, electrostatic, pi-sulfur, pi-pi and pi-alkyl interaction, respectively.

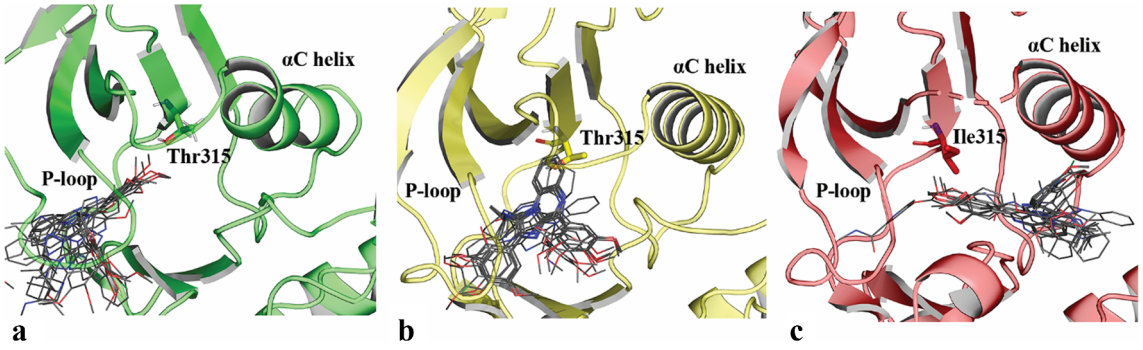

Fig. 4. Difference in docking location of synthesized compounds over DFG-in (a), DFG-out (b), and mutant T315I (c) active sites of ABL1.

Table 7
Re-docking results for wild type (DFG-in and DFG-out) and mutant T315I ABL1.

Ligand	Pdb id	Estimated free binding energy (kcal mol^{-1})		Hydrogen bond (Donor-Acceptor)	Electrostatic interaction
		H-bond + Vw	Electrostatic		
Dasatinib	2gqg	−9.92 −10.65	−1.35	N9-Thr315:OG1	–
VX-680	4zoq	−10.72 −12.22	−0.81	MET318:N -N20 H26 - Met318:O	–
DCC-2036	3qrj	−14.29 −16.31	−0.06	Met318:HN - N23 Asp381:HN - O63 N56 - Glu286:OE2 N60 - Glu286:OE2 N74 - Met318:O	Glu286:OE1 – quinazoline ring Glu286:OE2 – quinazoline ring Asp381:OD2 – quinazoline ring Asp381:OD2 – pyrazol ring

both variants have the same flexibility pattern at *N*-loop residues, while the wild-type shows higher flexibility at C-loop region specially at residue number 380 to 413 and 440 to 455 as compared to the mutant variant which are related to the activation loop region (Fig. 7).

In order to investigate binding stability of compound **6–34** in the active site of wild type and mutant variant, ligand positional RMSD were generated and investigated. Compound **6–34** showed slightly more and continues fluctuations in the size of 0.6–0.8 Å (Fig. 8a) for wild type and 0.6–1 Å for the mutant variant BCR-ABL complex (Fig. 8b). As shown in Fig. 8, the positional RMSD value of compound **6–34** in both types of ABL1 during the MD run was less than 2.0 Å, so the ligand was judged to be stable and this MD run regarded as a qualified run [32].

Comparing the structure of wild-type and the mutant variant ABL1 complexed with compound **6–34** after MD simulation revealed two important conformational differences. The first change has been detected in the *N*-lobe which shows upward shifting of αC helix motif in mutant rather than wild-type (Fig. 10a,b). The other difference of the mutant variant structural feature is in the C-lobe and is switching off Phe382 away from αC helix entrance gate and shifting toward the ATP binding loop (Fig. 9c, d). Consequently, the orientation of the proximal

Table 8
Docking results of synthesized compounds over wild type (DFG-in) ABL1 (2gqg).

Ligand	Final Intermolecular Energy (kcal mol^{-1})		Hydrogen bond (Donor-Acceptor)	Electrostatic	Hydrophobic
	H-bond + Vw	Electrostatic			
7	−11.76		Met318:HN-O34	–	Leu370, Tyr253,
	−11.77	+0.01	Asn322:HD22-N15		Leu248, VAL256
					ALA269
14	−12.09		Gln252:HN - O31	–	LEU248, TYR253
	−11.92	−0.17	Gln252:HN - O39		PHE317, ALA269
			Tyr253:HN - O39		LEU370
24	−11.21		N15-Leu248:O	–	LEU370, TYR253, PHE317, LEU248,
	−11.28	+0.07			VAL256, ALA269
32	−11.73		Gln252:HN-O28	Asp325:OD2-imidazol	TYR253, LEU248
	−11.55	−0.18	Tyr:HN-O28		LEU370, ARG367, GLY321
33	−13.12		Gln252:HN-O34	–	LEU248, TYR253, LEU370, VAL256,
	−13.05	−0.07	N15-Leu248:O		ALA269
34	−12.06		Gln252:HN-O32	–	LEU248, VAL256
	−11.81	−0.25	Tyr253:HN-O32		ALA269, LEU370
			Met318:HN-O36		
			H2-N13		
			(intramolecular)		
Staurosporin	−9.41			Asp325:OD2 Glu329:OD2-methyl	TYR253, TYR320, GLY321, LEU248
	−7.79	−1.62		amine	

Table 9
Docking results of synthesized compounds over wild type (DFG-out) ABL1 (4zog).

Ligand	Final Intermolecular Energy (kcal mol^{-1})		Hydrogen bond (Donor-Acceptor)	Electrostatic	hydrophobic
	H-bond + Vw	Electrostatic			
7	−11.23		LYS271:NZ-dimethoxy phenyl ring	LYS271:NZ- dimethoxy phenyl ring	TYR253, ALA269, LYS271, VAL256
	−11.22	−0.02			
14	−12.82		ASN322:N-O37	LYS271:NZ- dimethoxy phenyl ring	LYS271, ILE313, VAL256, TYR253, PHE382
			GLY383:N-O41		
	−12.62	−0.2			
24	−11.16		GLY383:HN-O31	LYS271:NZ- dimethoxy phenyl ring	LEU370, TYR253, VAL256, ALA269, LYS271
	−11.13	−0.03			
32	−12.31		GLY383:HN-O31	LYS271:NZ- dimethoxy phenyl ring	LEU370, TYR253, VAL256, ALA269, LYS271
	−12.25	−0.07			
33	−13.26		GLY383:HN-O31	LYS271:NZ- dimethoxy phenyl ring	LEU370, TYR253, VAL256, ALA269, LYS271, ILE313, MET318, PHE317
	−13.19	−0.07			
34	−12.08		GLY383:HN-O31	LYS271:NZ- dimethoxy phenyl ring	LEU370, TYR253, VAL256, ALA269, LYS271, ALA380
	−12.03	−0.05			
Staurosporin	−10.54		NH1 (from lactam ring)-GLU316:O	–	VAL299, LEU370,ALA380, ALA269,VAL256, TYR253, LEU248,
			C9-THR315:OG1		
	−10.59	+0.05			

part of activation loop changed relative to the αC helix. These conformational changes provided an open gate at the region between αC helix and the activation loop, so compound **6–34** entered and stabilized from the active site open gate close to the αC helix sides of the kinase.

Fig. 10 shows the bar chart which gives the fraction of the simulation time that compound **6–34** is in contact with various protein residues throughout the 40 ns MD trajectory of wild type and mutant variant. By comparing the interaction strength which is quantified by the frequency of occurrences in the trajectory it can revealed that during the course simulation, the most sustained interaction between **6** and **34** and the wild-type is hydrogen bond with Tyr253 and Asn322 (85% and 80% of the time, respectively), while these interactions is not seen with the mutant variant. As depicted in Fig. 12a and b however, compound **6–34** has more solvent exposure and hydrophobic interaction over mutant form than wild type. Notably, Although Thr315 provides significant water molecule bridges interaction over the wild type ABL1, the Ile mutation at the mentioned site contacts by less strength hydrophobic interaction with compound **6–34.**

3. Materials and methods

3.1. Characterization

IR spectra were taken using Nicolet FT-IR Magna 550 spectrographs. The samples were prepared for analysis by spectroscopic grade potassium bromide. Progress of the reactions was followed by TLC using silica gel SIL G/UV 254 plates. NMR spectra were run on a Bruker 500 MHz instrument respectively in CDCl3 and DMSO-d_6 with tetramethyl silane (TMS) as internal standard. Chemical shifts are given in δ scale in parts per million (ppm). Singlet (s), doublet (d), triplet (t), doublet of doublet (dd) and multiplet (m) are reported. Melting points were taken on a Kofler hot stage apparatus.

3.1.1. General procedure for the synthesis of N-alkyl-2, 4-diphenylimidazo [1, 2-a] quinoxalin-1-amine

To a round bottom flask containing DMF (10 mL), *o*-phenylenediamine (5 mmol), related benzaldehydes (5 mmol) and 4Å molecular

Table 10
Docking results of synthesized compounds over mutant T315I ABL1 (3qrj).

Ligand	Final Intermolecular Energy (Kcal mol^{-1})		Hydrogen bond	Electrostatic	Hydrophobic
	H-bond + Vw	Electrostatic			
7	−11.85		–	HIS361:NE2-quinoxaline ring	MET290, VAL299
	−11.80	−0.06		ASP381:OD2-imidazol ring	HIS361, LYS285
					LEU298, MET290
					ALA380, VAL289
					MET290, ILE315
14	−11.30		–	Asp381:OD1-trimethoxy phenyl ring	MET290, ILE293
	−11.25	−0.07		Asp381:OD2-imidazol ring	LEU298, VAL299
					ILE315, ALA380
24	−11.53		–	Glu286:OE1-phenyl ring	MET290, ILE293
	−11.50	−0.02		Asp381:OD2-imidazolo ring	LEU298, VAL299
					ILE315, ALA380
32	−13.01		–	GLU286:OE1-phenyl ring	MET290, ILE293LEU298, VAL299
	−12.96	−0.06		ASP381:OD2-imidazolo ring	ILE315, ALA380
33	−13.67		–	GLU286:OE1-phenyl ring	MET290, ILE293
	−13.61	−0.07		ASP381:OD2-imidazolo ring	LEU298, VAL299
					ILE315, ALA380, HIS361, PHE382
34	−12.49		–	GLU286:OE1-phenyl ring	ASP381, PHE382
	−12.42	−0.07		ASP381:OD2-imidazolo ring	MET290, ILE293
					LEU298, VAL299
					ILE315, ALA380
Staurosporin	−7.76		–	–	LEU248
	−6.96	−0.77			

sieve (100 mg) were added. The reaction mixture stirred at 50 °C for 4 h. and then, sodium cyanide (6 mmol) was added to the reaction mixture and stirred for more 12 h. The completion of the reaction was monitored by TLC. The reaction mixture was poured on ice water and allowed to precipitate. The precipitate was filtered and purified by column chromatography (hexane/ethyl acetate, 90:10 v/v).

To a mixture of 3-phenylquinoxalin-2-amine (compound 3 in Scheme 1) (2 mmol), related benzaldehydes (2 mmol) and isocyanide (2 mmol) was added ammonium chloride (0.25 mmol). The mixture was stirred at 150 °C for 24 h. The reaction performance was monitored by TLC. After the reaction completion, the product was purified by column chromatography (hexane/ethyl acetate, 90:10 v/v).

3.1.1.1. 2, 4-bis (4-chlorophenyl)-N-cyclohexylimidazo [1, 2-a] quinoxalin-1-amine ***(6–1)***. M.p. = 202–203 °C; IR (KBr): 3345, 2933, 1588 cm^{-1}; ^{1}H NMR ($CDCl_3$, 500 MHz): δ = 1.11–1.84 (10*H*, m), 2.99 (1H, m), 3.59 (1H, d, J = 7.0 Hz), 7.47 (2H, d, J = 8.0 Hz), 7.53 (2H, d, J = 7.5 Hz), 7.58 (2H, t, J = 5.0 Hz), 7.86 (2H, d, J = 7.5 Hz), 8.12 (1H, d, J = 7.5 Hz), 8.78 (2H, d, J = 8.0 Hz), 9.14 (1H, d, J = 7.5 Hz) ppm; ^{13}C NMR ($CDCl_3$, 125 MHz): δ = 24.89, 25.58, 33.52, 57.34, 116.13, 126.13, 127.40, 128.43, 128.95, 130.38, 130.41, 130.92, 131.36, 131.53, 132.59, 133.69, 134.70, 136.49, 136.68, 137.19,

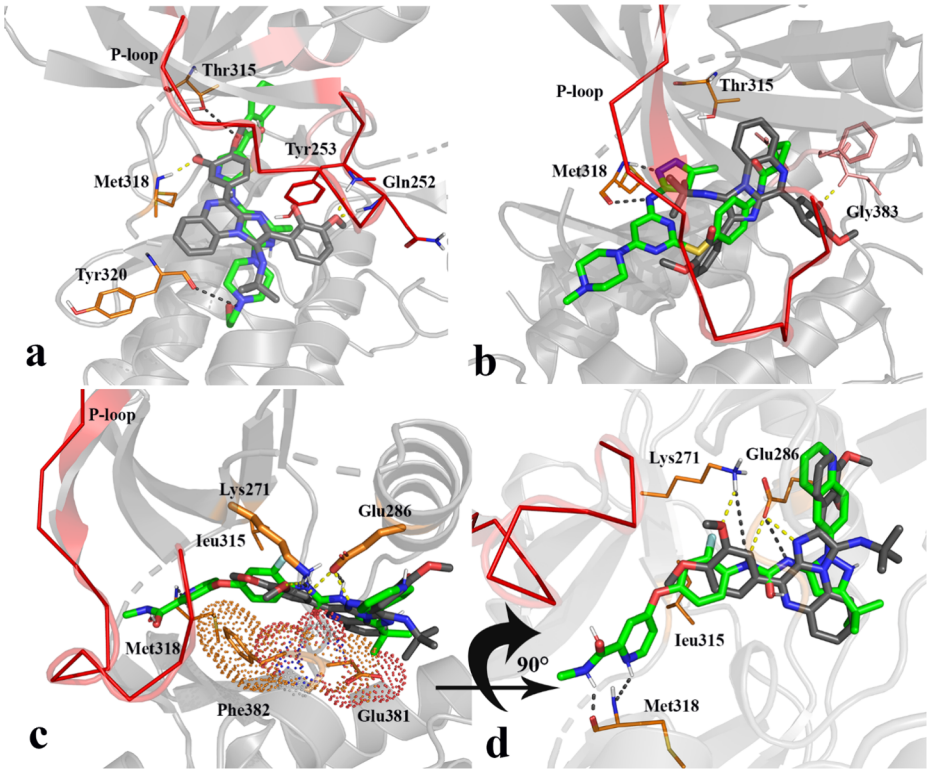

Fig. 5. Structural comparison of compound **6–34** and ABL1 inhibitor co-crystalized ligand. (a) Overlay of compound **6–34** (gray) with dasatinib (green). (b) Overlay of compound **6–34** with VX-680 (green). (c) Overlay of compound 6–34 (gay) with DCC-2036 (green). Hydrogen bonds within ABL1: compound **6–34** are depicted as dashed yellow lines, whereas those in ABL1:dasatinib, ABL1:VX-680, and ABL1:DCC-2036 are in black.

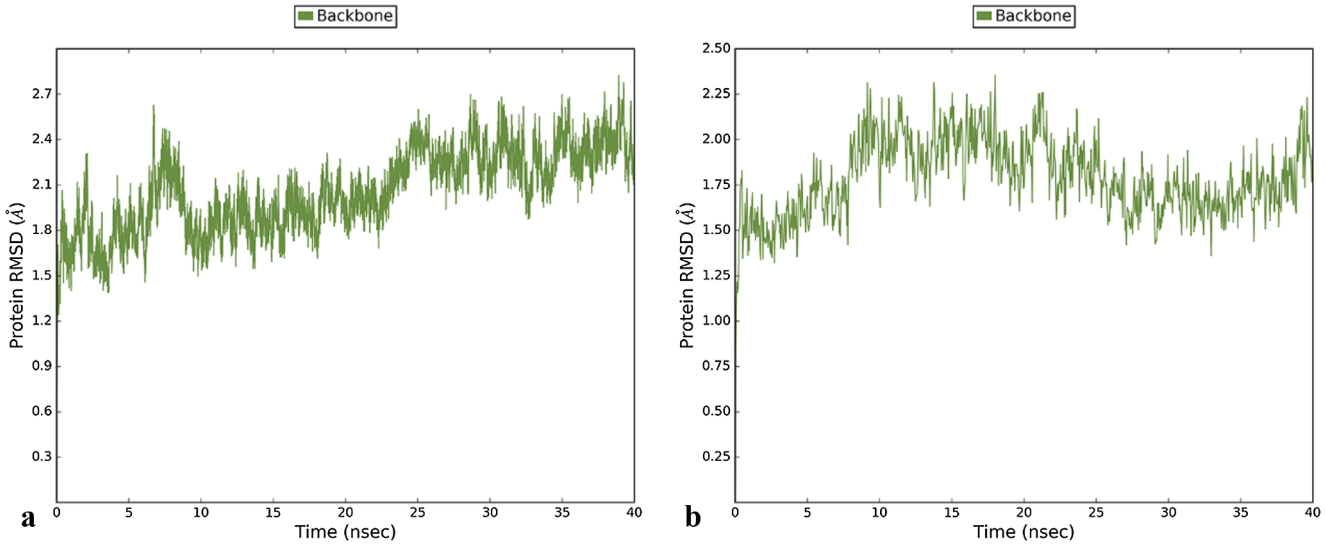

Fig. 6. Backbone RMSD representation of ABL1 for (a) wild type and (b) T315I mutant during 40 ns of simulation.

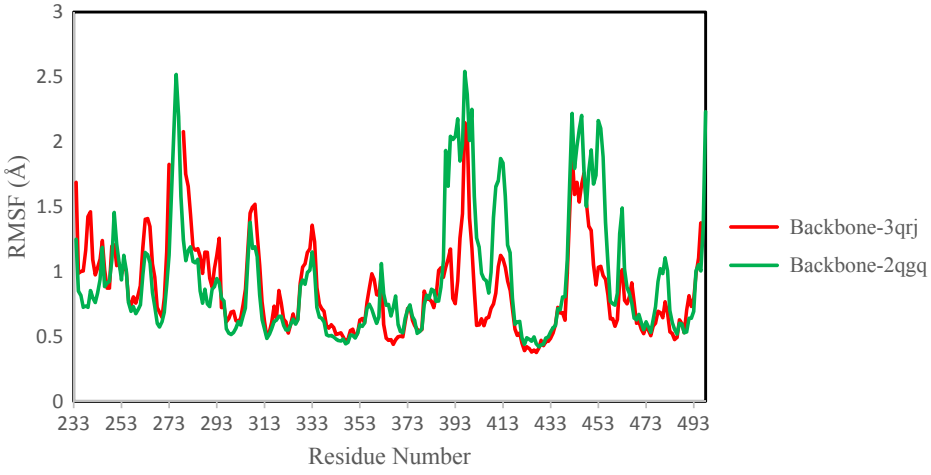

Fig. 7. Backbone RMSF representation of ABL1 for wild type and T315I mutant system during 40 ns of simulation.

148.65, 159.33 ppm. Anal. calcd. for $C_{28}H_{24}Cl_2N_4$: C, 69.00; H, 4.96; N, 11.49; Found: C, 69.11; H, 5.04; N, 11.57. HRMS: *m/z* $[M+H]^+$calcd for $C_{28}H_{24}Cl_2N_4$: 487.1456, found: 487.0128.

3.1.1.2. 4-(4-chlorophenyl)-N-cyclohexyl-2-(3, 4, 5-trimethoxyphenyl) imidazo[1,2-a]quinoxalin-1-amine ***(6–2)***. M.p. = 171–172 °C; IR (KBr): 3349, 2931, 1584 cm^{-1}; ^1H NMR ($CDCl_3$, 500 MHz): δ = 1.13–1.84 (10*H*, m), 3.04 (1H, m), 3.65 (1H, d, *J* = 6.5 Hz), 3.93–3.96 (9H, s), 7.12 (2H, s), 7.51 (2H, d, *J* = 8.0 Hz), 7.58 (2H, m), 8.12 (1H, d, *J* = 7.5 Hz), 8.79 (2H, d, *J* = 8.0 Hz), 9.13 (1H, d, *J* = 7.5 Hz) ppm; ^{13}C NMR ($CDCl_3$, 125 MHz): δ = 24.81, 25.61, 33.51, 56.41, 57.16, 61.00, 105.47, 116.16, 126.05, 127.29, 128.36, 128.71, 129.57, 130.25, 130.36,131.29, 131.39, 131.57, 133.58, 134.78, 136.40, 136.68, 148.52, 153.58 ppm. Anal. calcd. for $C_{31}H_{31}ClN_4O_3$: C, 68.56; H, 5.75; N, 10.32; Found: C, 68.61; H, 5.84; N, 10.38. HRMS: *m/z* $[M + H]^+$calcd for $C_{31}H_{31}ClN_4O_3$: 543.2163, found: 543.8993.

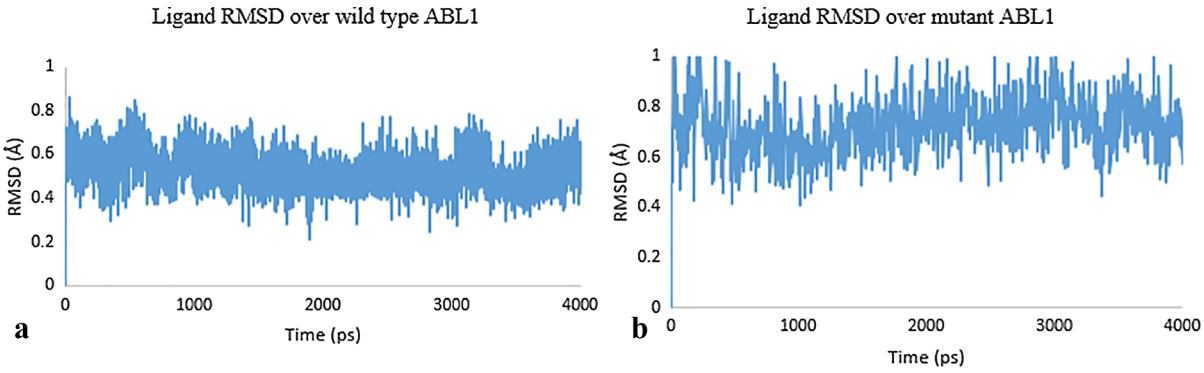

Fig. 8. Ligand positional RMSD of compound 6–34 over (a) wild type and (b) T315I mutant of ABL1 during 40 ns of simulation.

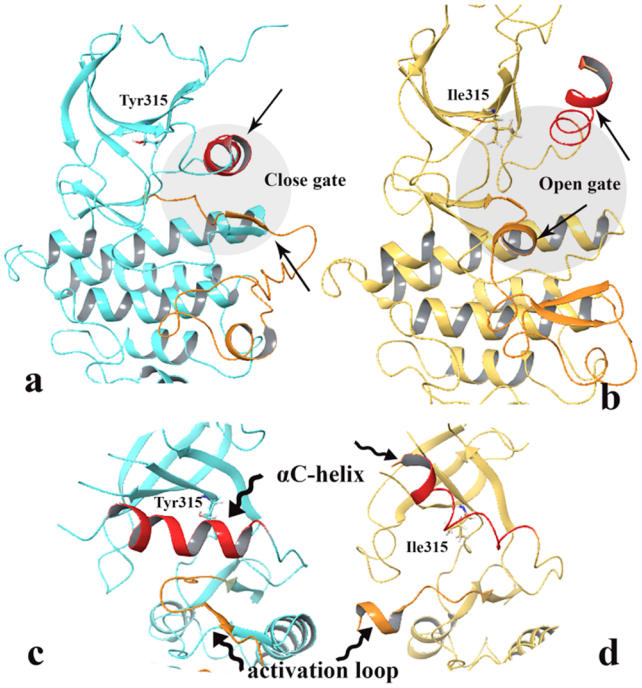

Fig. 9. Representation of wild type and mutant variant structure of ABL1 after 40 ns MD simulation, ABL1 wild-type (cyan) (a) and ABL1 T315I mutant (yellow) (b), 90 degrees left rotated of ABL1 active site of wild type (c) and mutant variant (d). αC helix and activation loop are in red and orange, respectively.

3.1.1.3. 4-(4-chlorophenyl)-N-cyclohexyl-2-(3, 4-dimethoxyphenyl) imidazo [1, 2-a] quinoxalin-1-amine ***(6–3)***. M.p. = 200–202 °C; IR (KBr): 3348, 2937, 1610 cm^{-1}; ^1H NMR ($CDCl_3$, 500 MHz): δ = 1.10–1.81 (10*H*, m), 3.00 (1H, m), 3.65 (1H, d, *J* = 7.0 Hz), 3.95–3.99 (6H, s), 6.99 (1H, d, *J* = 7.0 Hz), 7.37 (1H, s), 7.50 (2H, d, *J* = 8.0 Hz), 7.56 (2H, m), 8.11 (1H, d, *J* = 7.5 Hz), 8.29 (1H, d, *J* = 7.0 Hz), 8.80 (2H, d, *J* = 8.0 Hz), 9.15 (1H, d, *J* = 7.5 Hz) ppm; ^{13}C NMR ($CDCl_3$, 125 MHz): δ = 24.59, 24.84, 33.45, 55.94, 56.06, 57.14, 111.28, 111.43, 116.19, 120.16, 125.91, 126.88, 127.17, 128.32, 128.72, 130.27, 131.08, 131.35, 131.56, 133.53, 134.82, 136.30, 136.62, 138.14, 148.38, 148.95 ppm. Anal. calcd. for $C_{30}H_{29}ClN_4O_2$: C, 70.23; H, 5.70; N, 10.92; Found: C, 70.33; H, 5.81; N, 11.03. HRMS: *m/z* $[M + H]^+$calcd for $C_{30}H_{29}ClN_4O_2$: 513.2057, found: 513.9955.

3.1.1.4. 4-(4-chlorophenyl)-N-cyclohexyl-2-(4-methoxyphenyl) imidazo [1, 2-a] quinoxalin-1-amine ***(6–4)***. M.p. = 179–179 °C; IR (KBr): 3333, 2936, 1609 cm^{-1}; ^1H NMR ($CDCl_3$, 500 MHz): δ = 1.08–1.83 (10*H*, m), 2.98 (1H, m), 3.63 (1H, d, *J* = 7.5 Hz), 3.88 (3H, s), 7.03 (2H, d, *J* = 8.0 Hz), 7.52 (2H, d, *J* = 8.5 Hz), 7.56 (2H, t, *J* = 5.0 Hz), 7.81 (2H, d, *J* = 8.0 Hz), 8.11 (1H, d, *J* = 8.0 Hz), 8.80 (2H, d, *J* = 8.5 Hz), 9.17 (1H, d, *J* = 8.0 Hz) ppm; ^{13}C NMR ($CDCl_3$, 125 MHz): δ = 24.87, 25.60, 33.44, 55.30, 57.20, 114.19, 116.22, 125.84, 126.58, 127.13, 128.34, 128.79, 129.06, 130.23, 130.95, 131.56, 133.59, 134.86, 136.29, 136.63, 138.15, 148.40, 159.33 ppm. Anal. calcd. for $C_{29}H_{27}ClN_4O$: C, 72.11; H, 5.63; N, 11.60.; Found: C, 72.19; H, 5.71; N, 11.69. HRMS: *m/z* $[M + H]^+$calcd for $C_{29}H_{27}ClN_4O$: 483.1951, found: 483.1412.

3.1.1.5. 4-(4-chlorophenyl)-N-cyclohexyl-2-(4-fluorophenyl) imidazo [1, 2-a] qyinoxalin-1-amine ***(6–5)***. M.p. = 197–198; IR (KBr): 3336, 2925, 1595 cm^{-1}; ^1H NMR ($CDCl_3$, 500 MHz): δ = 1.10–1.82 (10*H*, m), 2.97 (1H, m), 3.58 (1H, d, *J* = 7.5 Hz), 7.18 (2H, t, $^3J_{H\text{-}H}$ = 8.0 Hz, $^3J_{H\text{-}F}$ = 8.5 Hz), 7.52 (2H, d, *J* = 8.0 Hz), 7.55–7.58 (2H, m), 7.87 (2H, t, $^3J_{H\text{-}H}$ = 8.0 Hz, $^4J_{H\text{-}F}$ = 6.5 Hz), 8.11 (1H, d, *J* = 8.0 Hz), 8.77 (2H, d, *J* = 8.0 Hz), 9.13 (1H, d, *J* = 8.0 Hz) ppm; ^{13}C NMR ($CDCl_3$, 125 MHz): δ = 24.85, 25.57, 33.46, 57.24, 115.63, 115.80, 116.11, 126.04, 127.33, 128.40, 128.74, 129.53, 130.20, 131.19, 131.44 ($^2J_{C\text{-}F}$ = 22.5 Hz), 133.73, 134.73, 136.43, 136.64, 137.44, 148.56, 162.45 ($^1J_{C\text{-}F}$ = 250 Hz) ppm. Anal. calcd. for $C_{28}H_{24}ClFN_4$: C, 71.41; H, 5.14; N, 11.90; Found: C, 71.51; H, 5.24; N, 12.01. HRMS: *m/z* $[M + H]^+$calcd for $C_{28}H_{24}ClFN_4$: 471.1752, found: 470.7887.

3.1.1.6. N-(tert-butyl)-4-(4-chlorophenyl)-2-(3, 4, 5-trimethoxyphenyl) imidazo [1, 2-a] quinoxalin-1-amine ***(6–6)***. M.p. = 174–175 °C; IR (KBr): 3352, 2974, 1585 cm^{-1}; ^1H NMR ($CDCl_3$, 500 MHz): δ = 1.02 (9H, s), 3.46 (1H, s), 3.91–3.96 (9H, s), 7.03 (2H, s), 7.52 (2H, d, *J* = 8.0 Hz), 7.54–7.57 (2H, m), 8.11 (1H, d, *J* = 4.5 Hz), 8.81 (2H, d, *J* = 8.0 Hz), 9.60 (1H, d, *J* = 4.5 Hz) ppm; ^{13}C NMR ($CDCl_3$, 125 MHz): δ = 29.73, 56.50, 57.71, 61.03, 106.38, 117.15, 126.10, 126.81, 128.39, 129.15, 130.28, 130.37, 131.43, 131.60, 133.98, 134.73, 136.41, 136.71, 138.27, 141.78, 148.46, 153.54 ppm. Anal. calcd. for $C_{29}H_{29}ClN_4O_3$: C, 67.37; H, 5.65; N, 10.84; Found: C, 67.43; H, 5.74; N, 10.92. HRMS: *m/z* $[M + H]^+$calcd for $C_{29}H_{29}ClN_4O_3$: 517.2006, found: 517.1574.

3.1.1.7. N-(tert-butyl)-4-(4-chlorophenyl)-2-(3, 4-dimethoxyphenyl) imidazo [1, 2-a] quinoxalin-1-amine ***(6–7)***. M.p. = 239–241 °C; IR (KBr): 3332, 2968, 1611 cm^{-1}; ^1H NMR ($CDCl_3$, 500 MHz): δ = 0.99 (9H, s), 3.48 (1H, s), 3.94–3.99 (6H, s), 6.95 (1H, d, *J* = 8.0 Hz), 7.29 (1H, d, *J* = 8.0 Hz), 7.41 (1H, s), 7.51–7.51 (4H, m), 8.10 (1H, d,

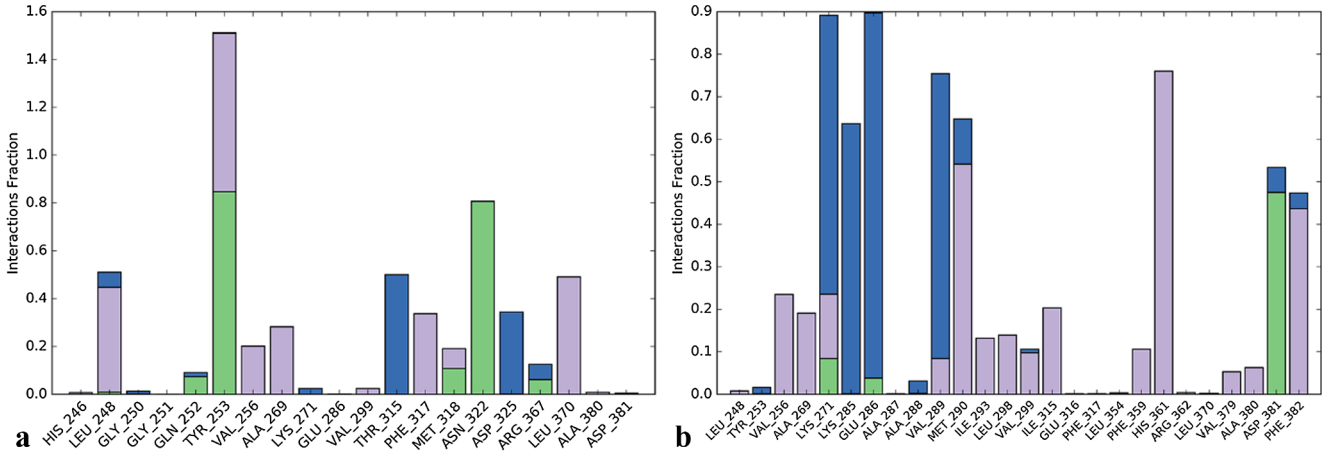

Fig. 10. Interaction frequencies of the non-bonding interactions between compound **6–34** and (a) wild type ABL1 and (b) T315I mutant variant during 40 ns. H-bond, hydrophobic, and water bridge interactions are in green, purple, and blue color, respectively.

J = 7.5 Hz), 8.81 (1H, d, J = 8.0 Hz), 9.61 (1H, d, J = 7.5 Hz) ppm; ^{13}C NMR ($CDCl_3$, 125 MHz): δ = 29.69, 55.94, 56.15, 57.61, 111.14, 112.16, 117.17, 121.09, 125.95, 126.69, 127.64, 128.35, 129.19, 130.05, 130.19, 130.31, 131.43, 131.59, 133.95, 134.79, 136.34, 136.68, 141.66, 148.34 ppm. Anal. calcd. for $C_{28}H_{27}ClN_4O_2$: C, 69.06; H, 5.59; N, 11.50; Found: C, 69.16; H, 5.64; N, 11.58. HRMS: m/z $[M + H]^+$calcd for $C_{28}H_{27}ClN_4O_2$: 487.1901, found: 486.8207.

3.1.1.8. N-(tert-butyl)-4-(4-chlorophenyl)-2-(4-methoxyphenyl) imidazo [1, 2-a] quinoxalin-1-amine ***(6–8)***. M.p. = 176–178 °C; IR (KBr): 3348, 2968, 1626 cm^{-1}; ^{1}H NMR ($CDCl_3$, 500 MHz): δ = 1.00 (9H, s), 3.46 (1H, s), 3.88 (3H, s), 7.03 (2H, d, J = 8.0 Hz), 7.52–7.55 (4H, m), 7.75 (2H, d, J = 8.0 Hz), 8.11 (1H, d, J = 7.5 Hz), 8.81 (2H, d, J = 8.0 Hz), 9.64 (1H, d, J = 7.5 Hz) ppm; ^{13}C NMR ($CDCl_3$, 125 MHz): δ = 27.74, 29.73, 57.33, 117.23, 126.06, 126.73, 127.95, 128.44, 128.61, 129.35, 130.27, 130.31, 130.42, 131.44, 131.64, 134.14, 134.76, 134.82, 136.46, 136.78, 141.73 ppm. Anal. calcd. for $C_{27}H_{25}ClN_4O$: C, 70.97; H, 5.51; N, 12.26; Found: C, 71.11; H, 5.64; N, 12.38. HRMS: m/z $[M + H]^+$calcd for $C_{27}H_{25}ClN_4O_2$: 457.1795, found: 456.1406.

3.1.1.9. N-(tert-butyl)-4-(4-chlorophenyl)-2-phenylimidazo [1, 2-a] quinoxalin-1-amine ***(6–9)***. M.p. = 212–213 °C; IR (KBr): 3351, 2955, 1587 cm^{-1}; ^{1}H NMR ($CDCl_3$, 500 MHz): δ = 0.99 (9H, s), 3.54 (1H, s), 7.38 (1H, t, J = 7 Hz), 7.47–7.56 (6H, m), 7.82 (2H, d, J = 7.0 Hz), 8.11 (1H, d, J = 5.0 Hz), 8.82 (2H, d, J = 8.0 Hz), 9.64 (1H, d, J = 5.0 Hz) ppm; ^{13}C NMR ($CDCl_3$, 125 MHz): δ = 29.66, 57.74, 117.27, 126.03, 126.76, 127.98, 128.42, 128.64, 129.31, 130.23, 130.35, 131.46, 131.61, 134.18, 134.78, 134.84, 136.42, 136.73, 141.75, 148.57 ppm. Anal. calcd. for $C_{26}H_{23}ClN_4$: C, 73.14; H, 5.43; N, 13.12; Found: C, 73.23; H, 5.54; N, 13.23. HRMS: m/z $[M + H]^+$calcd for $C_{26}H_{23}ClN_4$: 427.1689, found: 426.4635.

3.1.1.10. 4-(4-chlorophenyl)-N-cyclohexyl-2-phenyl) imidazo [1, 2-a] qyinoxalin-1-amine ***(6–10)***. M.p. = 211–212 °C; IR (KBr): 3341, 2927, 1594 cm^{-1}; ^{1}H NMR ($CDCl_3$, 500 MHz): δ = 1.08–1.83 (10*H*, m), 2.98 (1H, m), 3.70 (1H, d, J = 7.5 Hz), 7.38 (1H, t, J = 7.0 Hz), 7.48–7.56 (6H, m), 7.87 (2H, d, J = 7.0 Hz), 8.10 (1H, d, J = 7.5 Hz), 7.80 (2H, d, J = 8.0 Hz), 9.15 (1H, d, J = 7.5 Hz) ppm; ^{13}C NMR ($CDCl_3$, 125 MHz): δ = 24.86, 25.57, 33.41, 57.26, 116.23, 125.94, 127.20, 127.76, 128.36, 128.73, 129.41, 130.13, 130.24, 131.39, 131.55, 133.71, 134.02, 134.80, 136.35, 136.63, 138.08, 148.55 ppm. Anal. calcd. for $C_{28}H_{25}ClN_4$: C, 74.24; H, 5.56; N, 12.37; Found: C, 74.31; H, 5.64; N, 12.46. HRMS: m/z $[M + H]^+$calcd for $C_{28}H_{25}ClN_4$: 453.1846, found: 452.1356.

3.1.1.11. N-(tert-butyl)-2, 4-bis (4-chlorophenyl)-2-phenylimidazo [1, 2-a] quinoxalin-1-amine ***(6–11)***. M.p. = 214–216 °C; IR (KBr): 3378, 2923, 1592 cm^{-1}; ^{1}H NMR ($CDCl_3$, 500 MHz): δ = 0.99 (9H, s), 3.42 (1H, s), 7.45 (2H, d, J = 8.0 Hz), 7.51–7.56 (4H, m), 7.78 (2H, d, J = 8.0 Hz), 8.09 (1H, t, J = 5.0 Hz), 8.79 (2H, d, J = 8.0 Hz), 9.58 (1H, t, J = 5.0 Hz) ppm; ^{13}C NMR ($CDCl_3$, 125 MHz): δ = 29.75, 57.78, 117.12, 126.15, 126.88, 128.43, 128.83, 129.20, 129.78, 130.30, 130.39, 131.49, 133.36, 133.90, 134.26, 134.66, 136.52, 136.73, 140.59, 148.54 ppm. Anal. calcd. for $C_{26}H_{22}Cl_2N_4$: C, 67.68; H, 4.81; N, 12.14; Found: C, 67.76; H, 4.89; N, 12.25. HRMS: m/z $[M + H]^+$calcd for $C_{26}H_{22}Cl_2N_4$: 461.1300, found: 461.9944.

3.1.1.12. N-cyclohexyl-2,4-bis(3,4,5-trimethoxyphenyl)imadazo[1,2-a] quinoxalin-1-amine ***(6–12)***. M.p. = 203–204 °C; IR (KBr): 3335, 2925, 1612 cm^{-1}; ^{1}H NMR ($CDCl_3$, 500 MHz): δ = 1.13–2.03 (10*H*, m), 3.09 (1H, m), 3.61 (1H, m), 3.94–4.03 (18H, s), 7.23 (2H, s), 7.57 (2H, m), 8.14 (1H, m), 8.27 (2H, s), 9.15 (1H, m) ppm; ^{13}C NMR ($CDCl_3$, 125 MHz): δ = 24.82, 25.65, 33.53, 56.15, 56.25, 57.17, 60.92, 61.01, 105.00, 107.73, 116.09, 125.96, 127.02, 128.68, 129.76, 130.26, 130.91, 131.52, 133.78, 136.68, 137.67, 138.12, 140.26, 148.79, 152.83, 153.49 ppm. Anal. calcd. for $C_{34}H_{38}N_2O_6$: C, 68.21; H, 6.40; N, 9.36; Found: C, 68.32; H, 6.49; N, 9.47. HRMS: m/z $[M + H]^+$calcd for $C_{34}H_{38}N_4O_6$: 599.2869, found: 599.0741.

3.1.1.13. N-(tert-butyl)-2, 4-bis (3, 4, 5-trimethoxyphenyl)imidazo[1,2-a] quinoxalin-1-amine ***(6–13)***. M.p. = 208.7–209.7 °C; IR (KBr): 3387, 2925, 1586 cm^{-1}; ^{1}H NMR ($CDCl_3$, 500 MHz): δ = 1.05 (9H, s), 3.44 (1H, s), 3.92–4.04 (18H, s), 7.10 (2H, s), 7.55 (2H, t, J = 4.0 Hz), 8.13 (1H, d, J = 5.5 Hz), 8.29 (2H, s), 9.61 (1H, d, J = 5.5 Hz) ppm; ^{13}C NMR ($CDCl_3$, 125 MHz): δ = 29.66, 56.14, 56.32, 57.74, 60.91, 61.02, 106.01, 107.73, 117.05, 126.00, 126.54, 129.11, 129.87, 130.29, 130.51, 131.45, 134.14, 136.68, 138.33, 140.23, 141.26, 148.74, 152.83, 153.39 ppm. Anal. calcd. for $C_{32}H_{36}N_4O_6$: C, 67.12; H, 6.34; N, 9.78; Found: C, 67.21; H, 6.42; N, 9.86. HRMS: m/z $[M+H]^+$calcd for $C_{32}H_{36}N_4O_6$: 573.2713, found: 572.2761.

3.1.1.14. N-cyclohexyl-2-(3, 4-dimethoxyphenyl)-4-(3, 4, 5-trimethoxyphenyl) imadazo [1, 2-a] quinoxalin-1-amine ***(6–14)***. M.p. = 171–172 °C; IR (KBr): 3392, 2924, 1582 cm^{-1}; ^{1}H NMR ($CDCl_3$, 500 MHz): δ = 1.07–1.83 (10*H*, m), 3.01 (1H, m), 3.60 (1H, d, J = 6.5 Hz), 3.95–4.04 (15H, s), 6.95 (1H, d, J = 8.0 Hz), 7.40 (1H, d, J = 8.0 Hz), 7.541–7.570 (2H, m), 7.58 (1H, s), 8.12 (1H, t, J = 4.5 Hz), 8.27 (2H, s), 9.15 (1H, t, J = 4.5 Hz) ppm; ^{13}C NMR ($CDCl_3$, 125 MHz): δ = 24.83, 25.60, 33.42, 55.80, 55.88, 56.11, 57.10, 60.88, 107.65, 111.01, 111.14, 116.12, 119.57, 125.79, 126.88, 127.07, 128.66, 130.09, 130.75, 131.58, 133.66, 136.59, 137.72, 140.11, 148.65, 148.77, 149.17, 152.77 ppm. Anal. calcd. for $C_{33}H_{36}N_4O_5$: C, 69.70; H, 6.38; N, 9.85; Found: C, 69.81; H, 6.47; N, 9.94. HRMS: m/z $[M + H]^+$calcd for $C_{33}H_{36}N_4O_5$: 568.2686, found: 539.1565.

3.1.1.15. N-(tert-butyl)-2-(3, 4-dimethoxyphenyl)-4-(3, 4, 5-trimethoxyphenyl) imadazo [1, 2-a] quinoxalin-1-amine ***(6–15)***. M.p. = 165–167 °C; IR (KBr): 3341, 2921, 1586 cm^{-1}; ^{1}H NMR ($CDCl_3$, 500 MHz): δ = 1.02 (9H, s), 3.57 (1H, s), 3.95–4.04 (15H, s), 6.95 (1H, d, J = 8.0 Hz), 7.32 (1H, d, J = 8.0 Hz), 7.48 (1H, s), 7.54–7.57 (2H, m), 8.13 (1H, d, J = 5.0 Hz), 8.28 (2H, s), 9.63 (1H, d, J = 5 Hz) ppm; ^{13}C NMR ($CDCl_3$, 125 MHz): δ = 29.71, 55.92, 56.16, 57.69, 60.91, 61.03, 107.73, 111.01, 111.84, 117.13, 120.74, 125.89, 126.45, 127.84, 129.19, 129.81, 130.24, 131.55, 134.14, 136.70, 140.19, 141.24, 148.74, 148.98, 149.24, 152.85 ppm. Anal. calcd. for $C_{31}H_{34}N_4O_5$: C, 68.62; H, 6.32; N, 10.33; found: C, 68.71; H, 6.42; N, 10.42. HRMS: m/z $[M + H]^+$calcd for $C_{31}H_{34}N_4O_5$: 543.2607, found: 542.3171.

3.1.1.16. N-cyclohexyl-2-(3, 4-methoxyphenyl)-4-(3, 4, 5-trimethoxyphenyl) imadazo [1, 2-a] quinoxalin-1-amine ***(6–16)***. M.p. = 209–211 °C; IR (KBr): 3336, 2926, 1612 cm^{-1}; ^{1}H NMR ($CDCl_3$, 500 MHz): δ = 1.09–1.85 (10*H*, m), 2.99 (1H, m), 3.62 (1H, d, J = 7.0 Hz), 3.88–4.04 (12H, s), 7.02 (2H, d, J = 8.0 Hz), 7.55 (2H, t, J = 4.5 Hz), 7.84 (2H, d, J = 8.0 Hz), 8.13 (1H, d, J = 5.0 Hz), 8.24 (2H, s), 9.18 (1H, d, J = 5.0 Hz) ppm; ^{13}C NMR ($CDCl_3$, 125 MHz): δ = 24.91, 29.68, 33.47, 55.30, 56.24, 57.24, 60.91, 107.74, 114.17, 116.19, 125.79, 126.80, 126.89, 128.77, 030.07, 130.18, 130.74, 131.66, 133.77, 136.67, 137.86, 140.17, 148.94, 152.85, 159.24 ppm. Anal. calcd. for $C_{33}H_{36}$ N_4O_5: C, 69.70; H, 6.38; N, 9.85; Found: C, 69.81; H, 6.47; N, 9.96. HRMS: m/z $[M + H]^+$calcd for $C_{32}H_{34}N_4O_4$: 539.2658, found: 538.1494.

3.1.1.17. N-(tert-butyl)-2-(4-methoxyphenyl)-4-(3, 4, 5-trimethoxyphenyl) imadazo [1, 2-a] quinoxalin-1-amine ***(6–17)***. M.p. = 216–217. °C; IR (KBr): 3463, 2931, 1609 cm^{-1}; ^{1}H NMR ($CDCl_3$, 500 MHz): δ = 1.00 (9H, s), 3.49 (1H, s), 3.86–4.04 (12H, s), 7.00 (2H, d, J = 8.0 Hz), 7.53 (2H, t, J = 5.0 Hz), 7.76 (2H, d, J = 8.0 Hz), 8.10–8.13 (1H, m), 8.26 (2H, s), 9.62 (1H, d, J = 8.0 Hz), ppm; ^{13}C NMR ($CDCl_3$, 125 MHz): δ = 29.67, 55.26, 56.23, 57.59, 60.89, 107.76, 114.01, 117.12, 125.81, 126.39, 127.52, 129.22, 129.50, 129.71, 130.21, 131.59, 134.17, 136.69, 140.17,

141.26, 148.85, 152.85, 159.35 ppm. Anal. calcd. for $C_{30}H_{32}N_4O_4$: C, 70.29; H, 6.29; N, 10.93; Found: C, 70.41; H, 6.44; N, 11.08. HRMS: *m/z* $[M + H]^+$calcd for $C_{30}H_{32}N_4O_4$: 513.2502, found512.4182.

3.1.1.18. N-cyclohexyl-2-phenyl-4-(3, 4, 5-trimethoxyphenyl) imadazo [1, 2-a] quinoxalin-1-amine ***(6–18)***. M.p. = 220–221 °C; IR (KBr): 3324, 2928, 1580 cm^{-1}; ^1H NMR ($CDCl_3$, 500 MHz): δ = 1.09–1.85 (10*H*, m), 3.01 (1H, m), 3.71 (1H, d, *J* = 7.5 Hz), 3.95–4.04 (9H, s), 7.37 (1H, t, *J* = 7.0 Hz), 7.49 (2H, t, *J* = 7.0 Hz), 7.56 (2H, d, *J* = 3.5 Hz), 7.91 (2H, d, *J* = 7.0 Hz), 8.14 (1H, d, *J* = 4.5 Hz), 8.25 (2H, s), 9.17 (1H, d, *J* = 4.5 Hz) ppm; ^{13}C NMR ($CDCl_3$, 125 MHz): δ = 24.87, 25.59, 33.41, 56.22, 57.28, 60.89, 107.69, 116.18, 125.88, 126.96, 127.47, 127.62, 128.70, 129.74, 130.12, 131.57, 133.56, 133.88, 134.21, 136.66, 137.73, 140.18, 149.09, 152.85 ppm. Anal. calcd. for $C_{31}H_{32}N_4O_3$: C, 73.21; H, 6.34; N, 11.02; Found: C, 73.32; H, 6.45; N, 11.13. HRMS: *m/z* $[M+H]^+$calcd for $C_{31}H_{32}N_4O_3$: 509.2552, found: 508.2108.

3.1.1.19. N-cyclohexyl-4-phenyl-2-(3, 4, 5-trimethoxyphenyl) imadazo [1, 2-a] quinoxalin-1-amine ***(6–19)***. M.p. = 186–187 °C; IR (KBr): 3315, 2930, 1579 cm^{-1}; ^1H NMR ($CDCl_3$, 500 MHz): δ = 1.13–1.86 (10*H*, m), 3.06 (1H, m), 3.66 (1H, d, *J* = 5.0 Hz), 3.92–3.96 (9H, s), 7.14 (2H, s), 7.52–7.57 (5H, m), 8.15 (1H, d, *J* = 5.0 Hz), 8.75 (2H, d, *J* = 7.0 Hz), 9.15 (1H, d, *J* = 5.0 Hz) ppm; ^{13}C NMR ($CDCl_3$, 125 MHz): δ = 24.83, 25.65, 33.53, 56.42, 57.71, 61.00, 105.58, 116.13, 125.95, 127.08, 128.19, 128.88, 129.81, 130.14, 130.19, 130.34, 131.36, 131.59, 133.86, 136.32, 136.84, 138.51, 149.95, 153.58 ppm. Anal. calcd. for $C_{31}H_{32}N_4O_3$: C, 73.21; H, 6.34; N, 11.02; Found: C, 73.33; H, 6.48; N, 11.15. HRMS: *m/z* $[M+H]^+$calcd for $C_{31}H_{32}N_4O_3$: 509.2552, found: 508.8781.

3.1.1.20. N-(tert-butyl)-4-phenyl-2-(3, 4, 5-trimethoxyphenyl) imadazo [1, 2-a] quinoxalin-1-amine ***(6–20)***. M.p. = 179–180 °C; IR (KBr): 3335, 2926, 1581 cm^{-1}; ^1H NMR ($CDCl_3$, 500 MHz): δ = 1.02 (9H, s), 3.46 (1H, s), 3.90 (9H, s), 7.04 (2H, s), 7.54–7.55 (5H, m), 8.12 (1H, d, *J* = 5.0 Hz), 8.77 (2H, d, *J* = 7.0 Hz), 9.60 (1H, d, *J* = 5.0 Hz) ppm; ^{13}C NMR ($CDCl_3$, 125 MHz): δ = 29.73, 56.49, 57.64, 61.00, 106.45, 117.09, 125.33, 125.96, 126.56, 128.19, 129.14, 130.14, 130.19, 130.33, 130.53, 134.18, 136.33, 136.86, 138.46, 141.75, 149.96, 153.50 ppm. Anal. calcd. for $C_{29}H_{30}N_4O_2$: C, 72.18; H, 6.27; N, 11.61; Found: C, 72.38; H, 6.48; N, 11.92. HRMS: *m/z* $[M + H]^+$calcd for $C_{29}H_{30}N_4O_3$: 483.2396, found: 482.7970.

3.1.1.21. N-cyclohexyl-2-(3, 4-dimethoxyphenyl)-4-phenylimadazo [1, 2-a] quinoxalin-1-amine ***(6–21)***. M.p. = 171–173 °C; IR (KBr): 3386, 2931, 1610 cm^{-1} ; ^1H NMR ($CDCl_3$, 500 MHz): δ = 1.09–1.85 (10*H*, m), 3.02 (1H, m), 3.66 (1H, d, *J* = 7.0 Hz), 3.95–3.99 (6H, s), 6.98 (1H, d, *J* = 8.0 Hz), 7.39 (1H, d, *J* = 8.0 Hz), 7.51–7.57 (6H, m), 8.14 (1H, d, *J* = 7.0 Hz), 8.76 (2H, d, *J* = 7.5 Hz), 9.16 (1H, d, *J* = 7.0 Hz) ppm ; ^{13}C NMR ($CDCl_3$, 125 MHz): δ = 24.88, 25.65, 33.49, 55.97, 56.10, 57.18, 111.34, 111.60, 116.16, 120.22, 125.82, 126.98, 127.13, 128.17, 128.79, 130.14, 130.26, 131.00, 133.86, 136.47, 136.85, 138.16, 142.20, 148.94, 149.31, 149.98 ppm; MS (70 eV): *m/z* = 478.25 (M +). Anal. calcd. for $C_{30}H_{30}N_4O_2$: C, 75.29; H, 6.32; N, 11.71; Found: C, 75.38; H, 6.41; N, 11.82. HRMS: *m/z* $[M+H]^+$calcd for $C_{30}H_{30}N_4O_2$: 478.2369, found: 478.9040.

3.1.1.22. N-(tert-butyl)-2-(3, 4-dimethoxyphenyl)-4-phenylimadazo [1, 2-a] quinoxalin-1-amine ***(6–22)***. M.p. = 175–177 °C; IR (KBr): 3340, 2934, 1577 cm^{-1}; ^1H NMR ($CDCl_3$, 500 MHz): δ = 1.00 (9H,s), 3.50 (1H, s), 3.94–3.99 (6H, s), 6.96 (1H, d, *J* = 8.0 Hz), 7.30 (1H, d, *J* = 8.0 Hz), 7.43 (1H,s), 7.51–7.57 (5H, m), 8.13 (1H, t, *J* = 5.0 Hz), 8.77 (2H, d, *J* = 7.5 Hz), 9.63 (1H, t, *J* = 5.0 Hz) ppm; ^{13}C NMR ($CDCl_3$, 125 MHz): δ = 29.71, 55.95, 56.15, 57.61, 111.13, 112.23, 117.16, 121.11, 125.87, 126.50, 127.83, 128.20, 129.23, 129.98, 130.16, 130.29, 132.36, 134.19, 136.40, 136.87, 141.67, 149.07, 149.30, 149.92 ppm. Anal. calcd. for $C_{28}H_{28}N_4O_2$: C, 74.31; H, 6.24; N, 12.38; Found: C, 74.41; H, 6.34; N, 12.48. HRMS: *m/z* $[M + H]^+$calcd for $C_{28}H_{28}N_4O_4$: 453.2990, found: 452.9129.

3.1.1.23. N-cyclohexyl-2, 4-diphenylimadazo [1, 2-a] quinoxalin-1-amine ***(6–23)***. M.p. = 192–192 °C; IR (KBr): 3333, 2924, 1605 cm^{-1}; ^1H NMR ($CDCl_3$, 500 MHz): δ = 1.07–1.84 (10*H*, m), 2.99 (1H, m), 3.71 (1H, d, *J* = 8.0 Hz), 7.37 (1H, t, *J* = 7.25 Hz), 7.47–7.56 (7H, m), 7.89 (2H, d, *J* = 7.0 Hz), 8.13 (1H, t, *J* = 5.0 Hz), 8.77 (2H, d, *J* = 7.0 Hz), 9.17 (1H, d, *J* = 5.0 Hz) ppm; ^{13}C NMR ($CDCl_3$, 125 MHz): δ = 24.88, 25.61, 33.44, 57.27, 116.21, 125.85, 126.99, 127.66, 127.84, 128.19, 128.70, 128.83, 130.12, 130.17, 130.23, 131.53, 133.97, 134.21, 136.42, 136.84, 138.09, 150.15 ppm. Anal. calcd. for $C_{28}H_{26}N_4$: C, 80.35; H, 6.26; N, 13.39; Found: C, 80.43; H, 6.37; N, 13.48. HRMS: *m/z* $[M + H]^+$calcd for $C_{28}H_{26}N_4$: 419.2235, found: 418.9160.

3.1.1.24. N-(tert-butyl)-2, 4-diphenylimadazo [1, 2-a] quinoxalin-1-amine ***(6–24)***. M.p. = 197–199 °C; IR (KBr): 3330, 2986, 1608 cm^{-1}; ^1H NMR ($CDCl_3$, 500 MHz): δ = 0.99 (9H, s), 3.55 (1H, s), 7.37 (1H, t, *J* = 7.25 Hz), 7.48 (2H, t, *J* = 7.25 Hz), 7.51–7.57 (5H, m), 7.83 (2H, d, *J* = 7.5 Hz), 8.13 (1H, t, *J* = 5.0 Hz), 8.78 (2H, d, *J* = 7.5 Hz), 9.65 (1H, t, *J* = 5.0 Hz) ppm; ^{13}C NMR ($CDCl_3$, 125 MHz): δ = 29.67, 57.70, 117.22, 125.91, 126.53, 127.87, 128.22, 128.58, 128.65, 129.32, 130.17, 130.21, 130.31, 131.24, 135.00, 136.37, 136.91, 141.73, 150.10, 163.48 ppm. Anal. calcd. for $C_{26}H_{24}N_4$: C, 79.56; H, 6.16; N, 14.27; Found: C, 79.61; H, 6.24; N, 14.36. HRMS: *m/z* $[M + H]^+$calcd for $C_{26}H_{24}N_4$: 393.2079, found: 393.2103.

3.1.1.25. N-cyclohexyl-2-(4-fluorophenyl)-4-phenylimadazo [1, 2-a] quinoxalin-1-amine ***(6–25)***. M.p. = 201–203 °C; IR (KBr): 3367, 2929, 1605 cm^{-1}; ^1H NMR ($CDCl_3$, 500 MHz): δ = 1.11–1.83 (10*H*,m), 2.99 (1H, m), 3.58 (1H, d, *J* = 7.0 Hz), 7.18 (2H, t, $^3J_{H\text{-}H}$ = 8.0 Hz, $^3J_{H\text{-}F}$ = 8.25 Hz), 7.50–7.61 (5H, m), 7.88 (2H, t, $^3J_{H\text{-}H}$ = 8.0 Hz, $^4J_{H\text{-}F}$ = 6.5 Hz), 8.15 (1H, d, *J* = 5.5 Hz), 8.74 (2H, d, *J* = 7.0 Hz), 9.14 (1H, d, *J* = 8.5 Hz) ppm; ^{13}C NMR ($CDCl_3$, 125 MHz): δ = 24.87, 25.61, 33.48, 57.24, 115.58, 115.75, 116.09, 125.94, 127.11, 128.21, 128.78, 129.52, 129.58, 130.13 ($^2J_{C\text{-}F}$ = 22.5 Hz), 130.33, 131.10, 133.86, 136.35, 136.84, 137.45, 150.13, 162.43 ($^1J_{C\text{-}F}$ = 250 Hz) ppm. Anal. calcd. for $C_{28}H_{25}FN_4$: C, 77.04; H, 5.77; N, 12.83; Found: C, 77.13; H, 5.84; N, 12.91. HRMS: *m/z* $[M + H]^+$calcd for $C_{28}H_{25}FN_4$: 437.2141, found: 436.8382.

3.1.1.26. N-(tert-butyl)-2-(4-fluorophenyl)-4-phenylimadazo [1, 2-a] quinoxalin-1-amine ***(6–26)***. M.p. = 207–209 °C; IR (KBr): 3334, 2956, 1607 cm^{-1}; 1H NMR ($CDCl_3$, 500 MHz): δ = 0.96 (9H, s), 3.38 (1H, s), 7.14 (2H, t, $^3J_{H\text{-}H}$ = 8.0 Hz, $^3J_{H\text{-}F}$ = 8.5 Hz), 7.49–7.56 (5H, m), 7.79 (2H, t, $^3J_{H\text{-}H}$ = 8.0 Hz, $^4J_{H\text{-}F}$ = 6.5 Hz), 8.11 (1H, d, *J* = 7.0 Hz), 8.77 (2H, d, *J* = 7.5 Hz), 9.54 (1H, d, *J* = 8.0 Hz) ppm; ^{13}C NMR ($CDCl_3$, 125 MHz): δ = 29.69, 57.52, 115.42, 115.59, 117.02, 125.91, 126.55, 128.20, 129.17, 129.97, 130.11, 130.23, 130.29, 131.09, 134.32, 136.28, 136.83, 140.81, 149.94, 162.50 (1$J_{C\text{-}F}$ = 250 Hz) ppm. Anal. calcd. for $C_{26}H_{23}FN_4$: C, 76.08; H, 5.65; N, 13.65; Found: C, 76.16; H, 5.73; N, 13.74. HRMS: *m/z* $[M + H]^+$calcd for $C_{26}H_{23}FN_4$: 411.1986, found: 410.3782.

3.1.1.27. N-cyclohexyl-2-(4-methoxyphenyl)-4-phenylimadazo [1, 2-a] quinoxalin-1-amine ***(6–27)***. M.p. = 203.6–204.9 °C; IR (KBr): 3333, 2928, 1610 cm^{-1}; ^1H NMR ($CDCl_3$, 500 MHz): δ = 1.09–1.82 (10*H*, m), 2.99 (1H, m), 3.63 (1H, d, *J* = 6.5 Hz), 3.87 (3H, s), 7.02 (2H, d, *J* = 7.5 Hz), 7.55 (5H, m), 7.83 (2H, d, *J* = 7.5 Hz), 8.13 (1H, d, *J* = 5.0 Hz), 8.76 (2H, d, *J* = 7.0 Hz), 9.18 (1H, d, *J* = 5.0 Hz) ppm; ^{13}C NMR ($CDCl_3$, 125 MHz): δ = 24.90, 25.64, 33.47, 55.31, 57.21, 114.16, 116.18, 125.75, 126.78, 126.92, 128.17, 128.83, 129.05, 130.13, 130.21, 130.87, 133.89, 136.49, 136.82, 138.16, 141.12, 149.96, 159.28 ppm. Anal. calcd. for $C_{29}H_{28}N_4O$: C, 77.65; H, 6.29; N, 12.49; Found: C, 77.81; H, 6.44; N, 12.61. HRMS: *m/z*

$[M + H]^+$calcd for $C_{29}H_{28}N_4O$: 449.2341, found: 448.9950.

3.1.1.28. N-(tert-butyl)-2-(4-methoxyphenyl)-4-phenylimadazo[1,2-a] quinoxalin-1-amine ***(6–28)***. M.p. = 205–207 °C; IR (KBr): 3330, 2960, 1612 cm^{-1}; 1H NMR (CDCl3, 500 MHz): δ = 0.99 (9H, s), 3.46 (1H, s), 3.86 (3H, s), 7.01 (2H, d, J = 8.0 Hz), 7.51–7.56 (5H, m), 7.76 (2H, d, J = 8.0 Hz), 8.12 (1H, t, J = 4.5 Hz), 8.78 (2H, d, J = 7.5 Hz), 9.63 (1H, d, J = 5.0 Hz) ppm; 13C NMR (CDCl3, 125 MHz): δ = 29.73, 55.31, 57.56, 114.05, 117.16, 125.80, 126.45, 127.54, 128.19, 128.83, 129.30, 129.81, 130.17, 130.27, 132.08, 134.26, 136.43, 136.88, 141.60, 149.91, 159.42 ppm. Anal. calcd. For C27H26N4O: C, 76.75; H, 6.20; N, 13.26; Found: C, 76.83; H, 6.31; N, 13.38. HRMS: m/z $[M + H]^+$calcd for $C_{27}H_{26}N_4O_4$: 422.2182, found: 422.0198.

3.1.1.29. 2-(4-chlorophenyl)-N-cyclohexyl-4-phenylimidazo[1,2-a] quinoxalin-1-amine ***(6–29)***. M.p. = 203–204 °C; IR (KBr): V =3333, 2928, 1610 cm^{-1}; ^{1}H NMR ($CDCl_3$, 500 MHz): δ = 1.09–1.71 (10*H*, m), 2.82–2.84 (1H, m), 3.78 (1H, d, J = 6.0 Hz), 7.12 (2H, d, J = 8.0 Hz), 7.19–7.21 (5H, m), 7.48 (2H, d, J = 8.0 Hz), 8.01 (1H, t, J = 5.0 Hz), 8.63 (2H, d, J = 5.0 Hz), 9.19 (1H, m) ppm; ^{13}C NMR ($CDCl_3$, 125 MHz): δ = 24.45, 25.29, 33.56, 57.70, 111.83, 116.88, 117.02, 120.29, 120.63, 121.07, 121.16, 123.53, 123.64, 124.46, 124.64, 127.03, 129.75, 132.04, 132.18, 136.37, 140.75, 148.07 ppm. Anal. calcd. For $C_{28}H_{25}ClN_4$: C, 74.24; H, 5.56; N, 12.37; Found: C, 74.45; H, 6.82; N, 12.56.

3.1.1.30. N-(tert-butyl)-2-(4-chlorophenyl)-4-phenylimidazo[1,2-a] quinoxalin-1-amine ***(6–30)***. M.p. = 210–214 °C; IR (KBr): V = 3345, 2960, 1618 cm^{-1}; ^{1}H NMR ($CDCl_3$, 500 MHz): δ = 1.01 (9H, s), 3.62 (1H, s), 3.47 (1H, s), 7.07 (2H, d, J = 7.5 Hz), 7.31–7.36 (5H, m), 7.56 (2H, d, J = 5.5 Hz), 8.00 (1H, t, J = 5.0 Hz), 8.74 (2H, d, J = 7.5 Hz), 9.44 (1H, d, J = 4.0 Hz) ppm; ^{13}C NMR ($CDCl_3$, 125 MHz): δ = 29.18, 57.90, 110.96, 115.11, 118.46, 121.36, 122.02, 123.00, 125.09, 127.66, 127.90, 129.57, 130.20, 130.47, 133.13, 142.57, 143.84, 150.07, 150.20, 151.47 ppm. Anal. calcd. For $C_{26}H_{23}ClN_4$: C, 73.14; H, 5.43; N, 13.12; Found: C, 73.38; H, 5.72; N, 13.31.

3.1.1.31. 2-(1-(cyclohexylamino)-2-(3,4,5-trimethoxyphenyl)imidazo [1,2-a]quinoxalin-4-yl)-6-methoxyphenol ***(6–31)***. M.p. = 218–221 °C; IR (KBr): V = 3340, 2958, 1610 cm^{-1}; 1H NMR ($CDCl_3$, 500 MHz): δ = 1.13–1.64 (10*H*, m), 2.95 (1H, m), 3.66 (1H, d, J = 6.0 Hz), 3.96–4.07 (12H, m), 5.90 (s, 1H, OH), 6.99 (1H, d, J = 8.0 Hz), 7.10 (2H, s), 7.41 (1H, d, J = 7.5 Hz), 7.55 (1H, m), 8.11 (1H, d, J = 5.0 Hz), 8.51 (2H, d, J = 7.5 Hz), 9.12 (1H, d, J = 5.0 Hz) ppm; ^{13}C NMR ($CDCl_3$, 125 MHz): δ = 24.81, 29.70, 33.50, 55.92, 56.26, 57.11, 60.97, 105.15, 112.74, 114.19, 116.05, 119.11, 123.95, 124.41, 125.87, 126.63, 128.53, 128.62, 129.82, 130.00, 130.92, 133.76, 136.78, 137.63, 146.13 ppm. Anal. calcd. For $C_{32}H_{34}N_4O_5$: C, 69.30; H, 6.18; N, 10.10; Found: C, 69.48; H, 6.45; N, 10.24.

3.1.1.32. 2-(1-(tert-butylamino)-2-(3,4,5-trimethoxyphenyl)imidazo[1,2-a]quinoxalin-4-yl)-6-methoxyphenol ***(6–32)***. M.p. = 210–214 °C; IR (KBr): 3345, 2960, 1618 cm^{-1}; ^{1}H NMR ($CDCl_3$, 500 MHz): δ = 1.01 (9H, s), 3.62 (1H, s), 3.47 (1H, s), 3.91–4.07 (12H, m), 5.91 (1H, s, OH), 7.07–7.10 (3H, m), 7.51–7.56 (2H, m), 8.11 (1H, t, J = 4.0 Hz), 8.54–8.57 (2H, m), 9.60 (1H, d, J = 5.0 Hz) ppm; ^{13}C NMR ($CDCl_3$, 125 MHz): δ = 29.70, 55.30, 56.24, 57.24, 60.91, 106.11, 112.60, 114.14, 117.04, 124.49, 125.93, 128.97, 130.02, 130.74, 131.66, 133.77, 136.67, 137.86, 140.17, 148.94, 152.85, 159.30 ppm. Anal. calcd. for $C_{30}H_{32}N_4O_5$: C, 68.17; H, 6.10; N, 10.60; Found: C, 68.01; H, 5.98; N, 10.38. HRMS: m/z $[M + H]^+$calcd for $C_{30}H_{32}N_4O_5$: 529.2451, found: 528.0609.

3.1.1.33. 2-(1-(cyclohexylamino)-2-(3,4-dimethoxyphenyl)imidazo[1,2-a]quinoxalin-4-yl)-6-methoxyphenol ***(6–33)***. M.p. = 214–218 °C; IR (KBr): 3348, 2970, 1615 cm^{-1}; ^{1}H NMR ($CDCl_3$, 500 MHz): δ = 1.12–1.85 (10*H*, m), 3.01 (1H, m), 3.72 (1H, d, J = 7.5 Hz), 3.97–4.06 (9H, m), 5.68 (s, 1H, OH), 7.12 (1H, s), 7.38 (2H, d, J = 7.0 Hz), 7.50 (1H, t, J = 7.0 Hz), 7.58 (2H, d, J = 7.0 Hz), 8.01 (1H, t, J = 5.0 Hz), 8.61 (2H, m), 9.21 (1H, m) ppm; ^{13}C NMR ($CDCl_3$, 125 MHz): δ = 25.61, 26.25, 32.62, 55.69, 56.11, 57.70, 110.98, 115.18, 115.55, 115.67, 118.48, 121.36, 122.02, 123.01, 124.69, 127.88, 128.08, 128.68, 135.89, 142.74, 143.88, 152.24, 152.43, 153.48, 159.29 ppm. Anal. calcd. for $C_{31}H_{32}N_4O_4$: C, 70.97; H, 6.15; N, 10.68; Found: C, 71.15; H, 6.42; N, 10.80. HRMS: m/z $[M + H]^+$calcd for $C_{31}H_{32}N_4O_4$: 525.2502, found: 524.0280.

3.1.1.34. 2-(1-(tert-butylamino)-2-(3,4-dimethoxyphenyl)imidazo[1,2-a] quinoxalin-4-yl)-6-methoxyphenol ***(6–34)***. M.p. = 210–214 °C; IR (KBr): 3335, 2964, 1625 cm^{-1}; ^{1}H NMR ($CDCl_3$, 500 MHz): δ = 1.00 (9H, s), 3.48 (1H, s), 3.95–4.07 (9H, m), 5.91 (1H, s, OH), 6.98 (1H, s), 7.10 (1H, m), 7.27–7.31 (2H, m), 7.45 (1H, t, J = 7.0 Hz), 7.53 (1H, d, J = 7.0 Hz), 8.10 (1H, t, J = 5.0 Hz), 8.55–8.58 (2H, m), 9.63 (1H, m) ppm; ^{13}C NMR ($CDCl_3$, 125 MHz): δ = 29.70, 55.95, 56.20, 58.03, 111.05, 111.99, 112.68, 114.17, 117.12, 120.93, 124.49, 125.85, 126.12, 129.99, 135.89, 136.15, 147.76, 148.97, 156.16, 159.95 ppm. Anal. calcd. for $C_{29}H_{30}N_4O_4$: C, 69.86; H, 6.07; N, 11.24; Found: C, 71.15; H, 6.25; N, 11.43. HRMS: m/z $[M + H]^+$calcd for $C_{29}H_{30}N_4O_4$: 499.2345, found: 498.0599.

3.2. Biological evaluations

3.2.1. Cell culture

Human breast adenocarcinoma (MB-468, ATCC No. HTB-132), human embryonic kidney cells (Hek-293, ATCC No. CRL-1573) and human leukemia cell line (CCRF-CEM, ATCC No. CCL-119) were purchased from American Type Culture Collection. The cells were grown on 75 cm^2 cell culture flasks with RPMI-1640 medium for CCRF, DMEM for MB-468, Hek-293, supplemented with 10% fetal bovine serum (FBS), and 1% penicillin–streptomycin solution (10,000 units of penicillin and 10 mg of streptomycin in 0.9% NaCl) in a humidified atmosphere of 5% CO2, 95% air at 37 °C.

3.2.2. Cytotoxicity assay

Cytotoxic avtivity of the compounds was evaluated on three different human cancereous cell lines: breast cancer (MB-468), fetal kidney (Hek-293) and leukemia (CCRF-CEM). The cytotoxic activity of the synthesized compounds was studied by MTS method. MB-468 (5,000 cells), Hek-293 cells (5,000 cells), and CCRF-CEM cells (50,000 cells) were seeded in 0.1 mL per well in 96-well plates 24 h prior to the experiment. Cells were treated with Dox (5 μM) and DMSO (16.6%) as positive controls and compounds **6-(1–34)** (50 μM). Plates were incubated for 24 or 72 h at 37 °C in a humidified atmosphere of 5% CO2. Before adding MTS reagent, medium of MB-468 and Hek-293 was replaced with fresh medium. Then, cell viability was determined by measuring the fluorescence intensity of the formazan product at 490 nm using a SpectraMax M2 microplate spectrophotometer. The percentage of cell survival was calculated as (OD value of cells treated with the compounds)/(OD value of untreated cells) × 100. All the experiments were carried out in triplicate.

Compounds **6–5, 6–14, 6–32, 6–33,** and **6–34** were dissolved to a 5 mM stock in DMSO. Reference compound staurosporine was dissolved in DMSO to a 1 mM stock. Staurosporine was purchased from Sigma-Aldrich (Saint Louis, MI). Cell Titer-Glo® 2.0 Luminescent cell viability assay reagent was purchased from Promega (Madison, WI). K562, MCF 10A, and MDA-MB-468 cell lines were purchased from American Type Culture Collection (Manassas, VA). BV-173 cell line was purchased from Creative Bio-array (Shirley, NY). Cell culture mediums are outlined below in Table 11. All media are supplemented with 100 μg/ml of penicillin, and 100 μg/ml of streptomycin. Cultures were maintained at 37 °C in a humidified atmosphere of 5% CO_2 and 95% air.

Compounds **6–5**, **6–14**, **6–32**, **6–33**, **6–34** and the reference

Table 11
Complete Cell Culture Media.

Cell Line	Media
BV-173	RPMI + 20% FBS
K562	Iscove's DMEM + 10%FBS
MCF 10A	DMEM/F12 + 5% Horse Serum + 20 ng/ml EGF + 5 μg/ml hydrocortisone + 100 ng/ml Cholera Toxin + 10 μg/ml Insulin
MDA-MB-468	DMEM + 10%FBS

compound staurosporine were diluted in DMSO solution with 5-dose and 5 folded dilutions in a source plate starting at 5 mM for the each tested compounds and 1 mM for Staurosporine. 125 nL of each the tested compounds or 25 nL of staurosporine were delivered from the source plate to each well of a 384-well cell culture plate by Echo 550. 25 μl of respective culture medium containing 2,000 BV-173, K562, MCF 10A, or MDA-MB-468 cells were added to each of the cell culture in duplicates. Then, cells were incubated with the compounds at 37 °C, 5% CO2 for 96 h. 25 μl of Cell Titer Glo 2.0 reagent was added to each well. The contents were mixed on an orbital shaker for 2 min and incubated at room temperature for 15 min to stabilize the luminescent signal. Luminescence was recorded by Envision 2104 Multilabel Reader (PerkinElmer, Santa Clara, CA). The number of viable cells in culture was determined based on quantitation of the ATP present in each culture well. IC_{50} values were calculated using the GraphPad Prism 4 program based on a sigmoidal dose-response equation. After that, the IC_{50} curves were plotted.

3.2.3. Kinase assay

Compounds were tested against 3 kinases in duplicate. Compounds were tested in 5-dose IC_{50} mode with 5-fold serial dilution starting at 125 μM. Control compound, staurosporine, was tested in a 10-dose IC_{50} with 4-fold serial dilution starting at 20 μM. All kinase reactions were performed at 200 μM ATP. The compounds were pre-incubated with the enzyme and substrate mixture about 20 min. Then, ATP was added to start the reaction. The reaction was continued for 2 h at room temperature. The activities at the highest concentration of compounds were less than 65%. The detailed experimental procedure is provided here. Details of the kinases inhibition studies are shown in Table 12.

Base Reaction buffer was prepared from 20 mM Hepes (pH 7.5), 10 mM MgCl2, 1 mM EGTA, 0.02% Brij35, 0.02 mg/ml BSA, 0.1 mM Na3VO4, 2 mM DTT, and 1% DMSO. Required cofactors are added individually to each kinase reaction. Testing compounds were dissolved in 100% DMSO to a specific concentration. The serial dilution was conducted by epMotion 5070 in DMSO. The substrate was prepared in freshly prepared reaction buffer. The required cofactors were added to the above substrate solution. The kinase was added into the substrate solution. Then, the solution was gently mixed. The compounds in 100% DMSO were added into the kinase reaction mixture by Acoustic technology (Echo550; nanoliter range) and incubated for 20 min at room temperature. 32P-ATP (Specific activity 10 μCi/μl) was added into the reaction mixture to initiate the reaction. The mixture was incubated for 2 h at room temperature. The radioactivity was detected by filter-binding method. The kinase activity data were expressed as the percent remaining kinase activity in test samples compared to vehicle (dimethyl sulfoxide) reactions.

Table 12
kinase inhibition conditions.

Kinases	Kinase (Invitrogen) Cat#	Kinase Conc. in Reaction (nM)	Substrate	Substrate Conc. in Reaction
ABL1	PR4348B	0.25	ABLtide	20 μM
c-Src	P3044	0.6	pEY (mg/ml)	0.2 mg/ml

3.3. Molecular modeling

3.3.1. Target preparation

The structure of ABL1 in two conformations; active or phosphorylated (DFG-in) and inactive (DFG-out) and T315I mutant were retrieved from the Protein Data Bank with PDB ID; 2gqg, 4zoq, and 3qrj, respectively, which co-crystalized with dasatinib, VX-680, and DCC-2036, respectively (Fig. 11) [33,34].

In the first step of our study, all of the water molecules and co-crystallized ligands were removed. The pKa values of the residues in the enzyme were calculated to determine if any of them were likely to adopt nonstandard ionization states, using PROPKA 2.0 [35]. The side chains of the lysine, arginine, and histidine residues were protonated, while the carboxylic groups of glutamic acid and aspartic acid were deprotonated.

3.3.2. Description of the ABL1 active site

Fig. 12 shows the kinase domain and kinase domain active site of ABL1. The Abl kinase domain active site is located between N- and C-lobes. Both lobes contribute important conserved residues to the active site. The *N*-lobe is composed of 5 strands of β-sheet and a single α-helix called the αC helix (from Val280 to Lys291). Phosphate binding loop (P-loop) (from Met243 to Asp255), which is essential for coordination of the ATP is constructed by residues connecting strands β1 and β2 in the *N*-lobe. In contrast, the C-lobe is mainly helical and encompasses the peptide substrate binding site. Thr315 which lies in a hinge region between the N and C lobes of the many tyrosine kinase, known as the gatekeeper residue where it controls access to a hydrophobic pocket in the active site of kinases [36]. C-lobe includes of an activation loop which activated followed by Tyr393 phosphorylation and subsequently producing salt bridge interaction with Arg. The conserved DFG exists *N*-terminal to the activation loop, which its conformation relative to the active sites produced active (DFG-in) and inactive (DFG-out) form of ABL1. In DFG-in conformer, the orientation of Asp381 of the DFG motif is towards the active site, while in the DFG-out conformer, the aspartate moves away and Phe382 moves inward the active site [37].

3.3.3. Molecular docking

Autodock 4.2.6 program was utilized to determine the probable binding conformations of the compounds **6–32**, **6–33** and **6–34** over the tyrosine kinase DFG-in, DFG-out and mutant ABL1 complex active sites. AutoDockTools 1.5.2 (ADT) was used to prepare the input files. All water molecules were removed from the enzymes crystallographic structures, polar hydrogens were added and partial atomic charges were assigned by Gasteiger-united charges method [38]. For each ligand, nonpolar hydrogens were merged, Gasteiger charges were assigned, and rotatable bonds were setup. The structures were then saved in the corresponding pdbqt file required by Autodock. A grid box of 100 × 40 × 40 Å (x, y, and z) was created over the whole active site, at the center of −19.98, 16.89, and −6.88 with the spacing of 0.375 Å in each dimension to evaluate the ligand–protein interactions. AutoGrid 4.2.6 was used to calculate the grid potential maps. Of the three different search algorithms offered by AutoDock 4.2.6, the Lamarckian genetic algorithm (LGA) consisting of 100 runs, 25×10^6 energy evaluations, and 27,000 generations was applied [39]. Other docking parameters were set to default. Cluster analysis was performed on the docked results using a root mean square (RMS) tolerance of 2.0 Å.

3.3.4. Molecular dynamic simulation

Molecular Dynamics Simulations were performed using Gromacs 4.5.5. We evaluated the stability of the wild type and mutant variant of BCR-ABL and the best drug candidate; 6–34 from the experimental and docking study. Automated topology builder (ATB) [40] was used to generate the topology file for the selected compound in the framework of GROMOS 53A6 force-field [41]. The protein–ligand complexes were then solvated with TIP3P explicit water molecules and placed in the

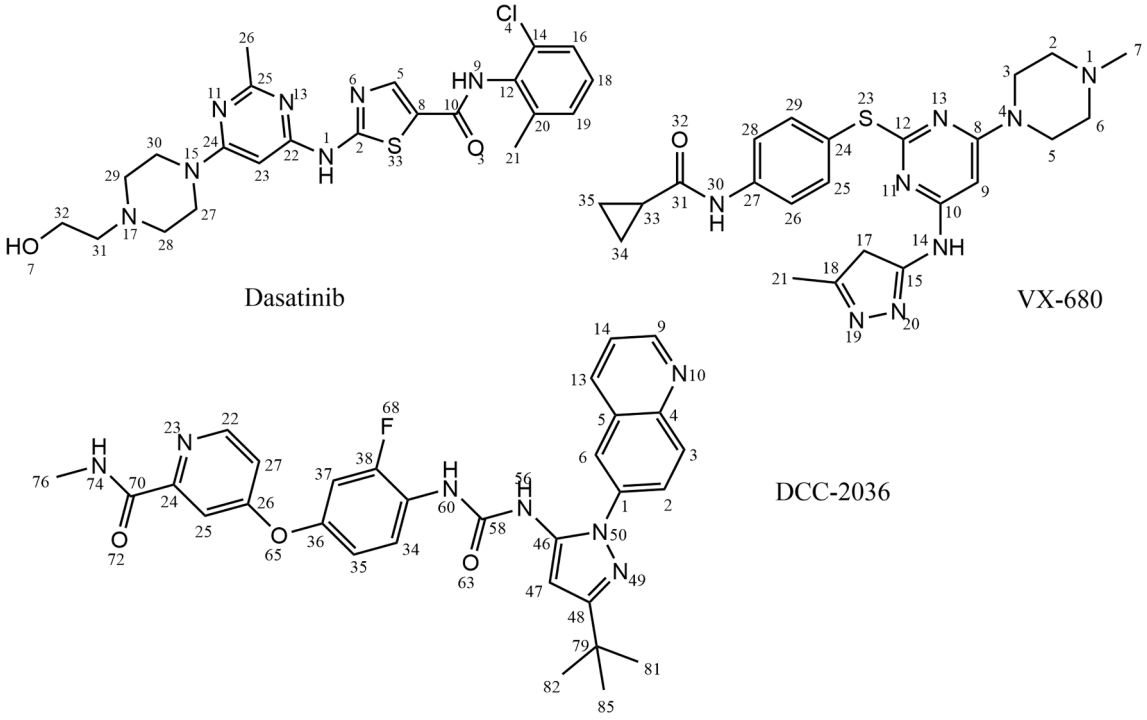

Fig. 11. 2D representation of co-crystalized dasatinib, VX-680, and DCC-2036 in the structure of ABL1; 2gqg, 4zoq, and 3qrj, respectively. Numbering is based on the original crystallographic pdb file.

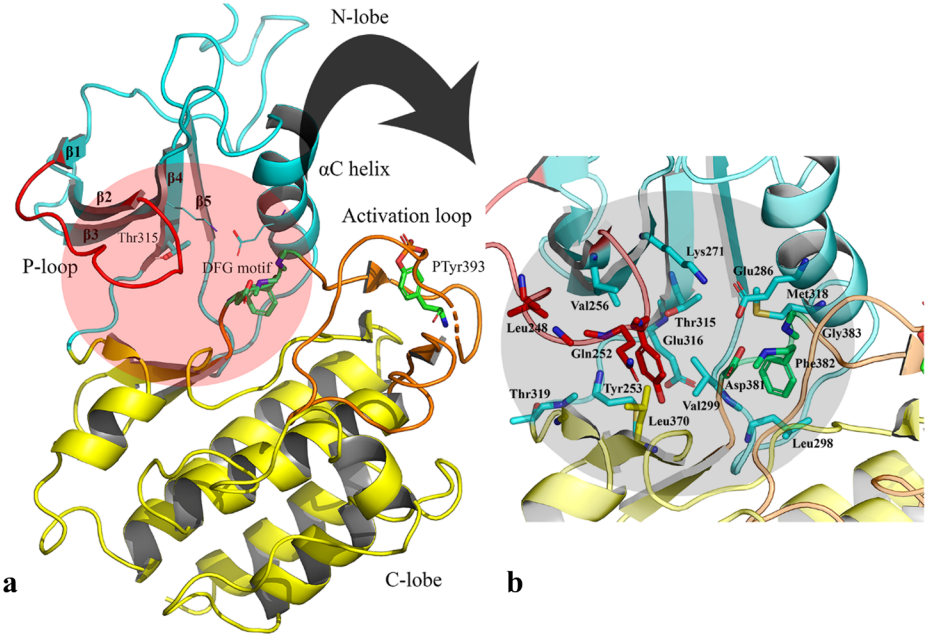

Fig. 12. Representation of ABL1 tyrosine kinase domain, The ABL1 consists of two lobes: *N*-lobe (*N*-terminal region) and C-lobe (Carboxyl terminal) which indicated in cyan and yellow color, respectively. P-loop, and activation loop are colored in red and orange, respectively (a). Close up (b) shows the active site.

center of a cubic box of size 24 × 24 × 24 Å. Minimum 1.0 Å distance was maintained between the protein and the edge of the simulation box so that protein can fully immerse with water and rotate freely. Then, Particle Mesh Ewald (PME) method [40] was used for the electrostatic energy calculation. It permits the use of the Ewald summation at a computational cost comparable to that of a simple truncation method of 10 A° or less, and the linear constraint solver (LINCS) algorithm was used for covalent bond constraints. Before minimization, the system was neutralized by adding $8Na^+$ ions. The steepest descent approach (1000 ps) was used for each protein–ligand complex for energy minimization. Further NVT was performed for 100 ps to equilibrate the system with protein and ligand for constant volume, pressure (1 atm) and temperature (300 K). The final MD run was set to 40000 ps for each protein-ligand complex.

4. Conclusions

In summary, a series of novel derivatives of N-alkyl-2,4-diphenylimidazo[1,2-*a*]quinoxalin-1-amine, were synthesized in two simple steps, and the final compounds were fully characterized by several

spectroscopy methods. The cytotoxicity of the products were evaluated against several human cancerous cell lines. In addition, the activities of the synthesized compounds were evaluated as kinase inhibitor. The results showed that 5-(1-(*tert*-butylamino)-2-(3, 4-dimethoxyphenyl) imidazo [1, 2-a] quinoxalin-4-yl)-2-methoxyphenol **(6–34)** was the most active compound in cell culture and enzyme assay studies.

The docking studies revealed that the synthesized compounds bound to three different forms of ABL1 (DFG-in motif, DFG-out motif and T315I mutant) whereas the bonding pattern over them are different, due to the different structure of the αC helix and activation loop. Modeling studies suggest that with this alternative conformation of Ile315 side chain, compound **6–34** is able to bind to the ATP site in a mutant form without serious steric clashes.

According to the analysis of the MD trajectories, different orientations have been detected among two structural parts of wild type and mutant variant ABL1. These regions include the αC helix from *N*-lobe and the activation loop from C-lobe which the last part consists of residues 393–413 and 433–453. The consequence of these changes produced an open gate at the region between αC helix and the activation loop in mutant form. As a result the binding location of the active compound 6–34 has been changed over two forms of tyrosin kinase with higher stability over the wild type rather than mutant ABL1 variant.

Acknowledgments

Tehran University of Medical Sciences & Health Services has supported this research (Grant Number: 91113022002).

Declaration of Competing Interest

The authors confirm that this article content has no conflict of interest.

References

[1] R.L. Siegel, K.D. Miller, A. Jemal, Cancer statistics, CA Cancer J. Clin. 66 (2016) 7–30.
[2] E. Pérez-Herrero, A. Fernández-Medarde, Advanced targeted therapies in cancer, drug nanocarriers, the future of chemotherapy, Eur. J. Pharm. Biopharm. 93 (2015) 52–79.
[3] P. Mahdaviani, S. Bahadorikhalili, M. Navaei-Nigjeh, S.Y. Vafaei, M. Esfandyari-Manesh, A.H. Abdolghaffari, Z. Daman, F. Atyabi, M.H. Ghahremani, M. Amini, A. Lavasanifar, Peptide functionalized poly ethylene glycol-poly caprolactone nanomicelles for specific cabazitaxel delivery to metastatic breast cancer cells, Mater. Sci. Eng. 80 (2017) 301–312.
[4] A. Kumar, I. Ahmad, B.S. Chhikara, R. Tiwari, D. Mandal, K. Parang, Synthesis of 3-phenylpyrazolopyrimidine-1, 2, 3-triazole conjugates and evaluation of their Src kinase inhibitory and anticancer activities, Bioorg. Med. Chem. Lett. 21 (2011) 1342–1346.
[5] A. Rafinejad, A. Fallah-Tafti, R. Tiwari, A.N. Shirazi, D. Mandal, A. Shafiee, K. Parang, A. Foroumadi, T. Akbarzadeh, 4-Aryl-4 H-naphthopyrans derivatives: one-pot synthesis, evaluation of Src kinase inhibitory and anti-proliferative activities, DARU J. Pharm. Sci. 20 (2012) 1–7.
[6] K. Chand, S. Prasad, R.K. Tiwari, A.N. Shirazi, S. Kumar, K. Parang, S.K. Sharma, Synthesis and evaluation of c-Src kinase inhibitory activity of pyridin-2 (1H)-one derivatives, Bioorg. Chem. 53 (2014) 75–82.
[7] R. Roskoski Jr, Janus kinase (JAK) inhibitors in the treatment of inflammatory and neoplastic diseases, Pharmacol. Res. 111 (2016) 784–803.
[8] P.K. Parikh, M.D. Ghate, Recent advances in the discovery of small molecule c-Met kinase inhibitors, Eur. J. Med. Chem. 143 (2018) 1103–1138.
[9] P. Manchanda, B. Parshad, A. Kumar, R.K. Tiwari, A.N. Shirazi, K. Parang, S.K. Sharma, Design, synthesis, and evaluation of the kinase inhibition potential of pyridylpyrimidinylaminophenyl derivatives, Arch. Pharm. 350 (2017) 3–4.
[10] V.J. Cee, F.J. Chavez, B. Herberich, B.A. Lanman, L.H. Pettus, A.B. Reed, B. Wu, R.P. Wurz, K.L. Andrews, J. Chen, D. Hickman, Discovery and Optimization of Macrocyclic Quinoxaline-pyrrolo-dihydropiperidinones as Potent Pim-1/2 Kinase Inhibitors, ACS Med. Chem. Lett. 7 (2016) 408–412.
[11] E.R. Kotb, M.A. Salama, M.A. Anwar, M.S. Soliman, Synthesis and reactions of some novel quinoxalines for anticancer evaluation, phosphorus, sulfur, silicon, Relat. Ele. 182 (2007) 1119–1130.
[12] J.A. Pereira, A.M. Pessoa, M.N. Cordeiro, R. Fernandes, C. Prudênc78io, J.P. Noronha, M. Vieira, Quinoxaline, its derivatives and applications: a state of the art review, Eur. J. Med. Chem. 5 (2015) 664–672.
[13] S.A. Galal, A.S. Abdelsamie, S.M. Soliman, J. Mortier, G. Wolber, M.M. Ali, H. Tokuda, N. Suzuki, A. Lida, R.A. Ramadan, H.I. El Diwani, Design, synthesis and structure–activity relationship of novel quinoxaline derivatives as cancer chemopreventive agent by inhibition of tyrosine kinase receptor, Eur. J. Med. Chem. 69 (2013) 115–124.
[14] H.Y. Liu, P.J. Wu, S.Y. Kuo, C.P. Chen, E.H. Chang, C.Y. Wu, Y.H. Chan, Quinoxaline-based polymer dots with ultrabright red to near-infrared fluorescence for in vivo biological imaging, J. Am. Chem. Soc. 137 (2015) 10420–10429.
[15] C. Patinote, N.B. Karroum, G. Moarbess, C. Deleuze-Masquefa, K. Hadj-Kaddour, P. Cuq, M. Diab-Assaf, I. Kassab, P.A. Bonnet, Imidazo [1, 2-a] pyrazine, Imidazo [1, 5-a] quinoxaline and Pyrazolo [1, 5-a] quinoxaline derivatives as IKK1 and IKK2 inhibitors, Eur. J. Med. Chem. 138 (2017) 909–919.
[16] A. Unzue, J. Dong, K. Lafleur, H. Zhao, E. Frugier, A. Caflisch, C. Nevado, Pyrrolo [3, 2-b] quinoxaline derivatives as types i1/2 and ii eph tyrosine kinase inhibitors: structure-based design, synthesis, and in vivo validation, J. Med. Chem. 57 (2014) 6834–6844.
[17] L.H. Pettus, K.L. Andrews, S.K. Booker, J. Chen, V.J. Cee, J.F. Chavez, Y. Chen, H. Eastwood, N. Guerrero, B. Herberich, D. Hickman, Discovery and optimization of quinazolinone-pyrrolopyrrolones as potent and orally bioavailable Pan-Pim kinase inhibitors, J. Med. Chem. 59 (2016) 6407–6430.
[18] F. Elahian, M. Akbari, M. Ghasemi, N. Behtooee, M. Taheri, M. Amini, Synthesis and anticancer activity of 2,4,5-triaryl imidazole derivatives, Lett. Drug Des. Discov. 11 (2014) 840–843.
[19] A. Unzue, K. Lafleur, H. Zhao, T. Zhou, J. Dong, P. Kolb, J. Liebl, S. Zahler, A. Caflisch, C. Nevado, Three stories on Eph kinase inhibitors: From in silico discovery to in vivo validation, Eur. J. Med. Chem. 112 (2016) 347–366.
[20] A. Assadieskandar, M. Amini, S.N. Ostad, G.H. Riazi, T. Cheraghi-Shavi, B. Shafiei, A. Shafiee, Design, synthesis, cytotoxic evaluation and tubulin inhibitory activity of 4-aryl-5-(3, 4, 5-trimethoxyphenyl)-2-alkylthio-1H-imidazole derivatives, Bioorg. Med. Chem. 21 (2013) 2703–2709.
[21] S. Tariq, K. Somakala, M. Amir, Quinoxaline: an insight into the recent pharmacological advances, Eur. J. Med. Chem. 143 (2017) 542–557.
[22] H.A. Abbas, A.R. Al-Marhabi, S.I. Eissa, Y.A. Ammar, Molecular modeling studies and synthesis of novel quinoxaline derivatives with potential anticancer activity as inhibitors of c-Met kinase, Bioorg. Med. Chem. 23 (2015) 6560–6572.
[23] Z. He, M. Bae, J. Wu, T.F. Jamison, Synthesis of highly functionalized polycyclic quinoxaline derivatives using visible-light photoredox catalysis, Angew. Chem. Int. Ed 53 (2014) 14451–14455.
[24] G. Rahimzadeh, S. Bahadorikhalili, E. Kianmehr, M. Mahdavi, Ionic liquid-functionalized magnetic nanostructures as an efficient catalyst for the synthesis of 6H-chromeno [4, 3-b] quinolin-6-ones, Mol. divers. 21 (2017) 597–609.
[25] C. Qi, H. Jiang, L. Huang, Z. Chen, H. Chen, DABCO-catalyzed oxidation of deoxybenzoins to benzils with air and one-pot synthesis of quinoxalines, Synthesis 3 (2011) 387–396.
[26] S. Ponra, K.C. Majumdar, Brønsted acid-promoted synthesis of common heterocycles and related bio-active and functional molecules, RSC Adv. 6 (2016) 37784–37922.
[27] C.S. Digwal, U. Yadav, A.P. Sakla, P.S. Ramya, S. Aaghaz, A. Kamal, $VOSO_4$ catalyzed highly efficient synthesis of benzimidazoles, benzothiazoles, and quinoxalines, Tetrahedron Lett. 57 (2016) 4012–4016.
[28] B. Roy, S. Ghosh, P. Ghosh, B. Basu, Graphene oxide (GO) or reduced graphene oxide (rGO): efficient catalysts for one-pot metal-free synthesis of quinoxalines from 2-nitroaniline, Tetrahedron Lett. 56 (2015) 6762–6767.
[29] M. Jeganathan, A. Dhakshinamoorthy, K. Pitchumani, One-pot synthesis of 2-substituted quinoxalines using K10-montmorillonite as heterogeneous catalyst, Tetrahedron Lett. 55 (2014) 1616–1620.
[30] K.S. Vadagaonkar, H.P. Kalmode, K. Murugan, A.C. Chaskar, I_2 catalyzed tandem protocol for synthesis of quinoxalines via sp^3, sp^2 and sp C-H functionalization, RSC Adv. 5 (2015) 5580–5590.
[31] K.D. Viswanadham, M.P. Reddy, P. Sathyanarayana, O. Ravi, R. Kant, S.R. Bathula, Iodine-mediated oxidative annulation for one-pot synthesis of pyrazines and quinoxalines using a multipathway coupled domino strategy, Chem. Commun. 50 (2014) 13517–13520.
[32] K. Liu, H. Kokubo, Exploring the stability of ligand binding modes to proteins by molecular dynamics simulations: a cross-docking study, J. Chem. Inf. Model. 57 (2017) 2514–2522.
[33] G.M. Morris, D.S. Goodsell, R.S. Halliday, R. Huey, W.E. Hart, R.K. Belew, A.J. Olson, Automated docking using a Lamarckian genetic algorithm and an empirical binding free energy function, J. Comput. Chem. 19 (1998) 1639–1662.
[34] M.F. Sanner, Python: a programming language for software integration and development, J. Mol. Graph. Model. 17 (1999) 57–61.
[35] D.C. Bas, D.M. Rogers, J.H. Jensen, Very fast prediction and rationalization of pKa values for protein–ligand complexes, Prot.: Struct. Funct. Bioinf. 73 (2008) 765–783.
[36] M. Azam, M.A. Seeliger, N.S. Gray, J. Kuriyan, G.Q. Daley, Activation of tyrosine kinases by mutation of the gatekeeper threonine, Nat. Struct. Mol. Biol. 15 (2008) 1109.
[37] Y. Shan, M.A. Seeliger, M.P. Eastwood, F. Frank, H. Xu, M.Q. Jensen, R.O. Dror, J. Kuriyan, D.E. Shaw, A conserved protonation-dependent switch controls drug

binding in the Abl kinase, Proc. Natl. Acad. Sci. U.S.A. 106 (2009) 139–144.
[38] O. Trott, A.J. Olson, AutoDock Vina: improving the speed and accuracy of docking with a new scoring function, efficient optimization, and multithreading, J. Comput. Chem. 31 (2010) 455–461.
[39] A.K. Malde, et al., An Automated Force Field Topology Builder (ATB) and Repository: Version 1.0, J. Chem. Theory Comput. 7 (2011) 4026–4037.
[40] C. Oostenbrink, A. Villa, A.E. Mark, W.F. van Gunsteren, A biomolecular force field based on the free enthalpy of hydration and solvation: the GROMOS force-field parameter sets 53A5 and 53A6, J. Comput. Chem. 25 (2004) 1656–1676.
[41] D. York, W. Yang, The fast Fourier Poisson method for calculating EWALD sums, J. Chem. Phys. 101 (1994) 3298–3300.
[42] D.A.E. Issa, N.S. Habib, A.E.A. Wahab, Design, synthesis and biological evaluation of novel 1,2,4-triazolo and 1,2,4-triazino[4,3-a]quinoxalines as potential anticancer and antimicrobial agents, Med. Chem. Commun. 6 (2015) 202–211.